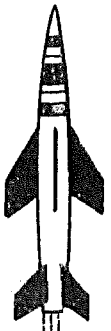

AEDC-TN-58-88
ASTIA DOCUMENT NO.:
AD-207771

cy 1



# BASE PRESSURE EFFECTS RESULTING FROM CHANGES IN TUNNEL PRESSURE RATIO IN A TRANSONIC WIND TUNNEL

By

L. E. Rittenhouse
PWT,ARO, Inc.



January 1959



ARNOLD ENGINEERING DEVELOPMENT CENTER
AIR RESEARCH AND DEVELOPMENT COMMAND
US AF

AEDC-TN-58-88
ASTIA DOCUMENT NO.:
AD-207771

# BASE PRESSURE EFFECTS RESULTING FROM CHANGES IN TUNNEL PRESSURE RATIO IN A TRANSONIC WIND TUNNEL

By

L. E. Rittenhouse

PWT, ARO, Inc.



January 1959

ARO Project No. 210503

Contract No. AF 40(600)-700 S/A 13(59-1)

AF - AEDC
Tullahoma, Tennessee

## CONTENTS



## ILLUSTRATIONS

Figure

## ABSTRACT

Effects of tunnel pressure ratio on test model base pressure measurements were determined for a finite- and infinite-length cylindrical body with both a blunt base and boattail afterbody throughout the Mach number range from 0.70 to 1.40 in the 1-Ft Transonic Tunnel, AEDC. The pressure ratios required to obtain correct base pressures independent of base station location are given for subsonic and supersonic tunnel operation under the conditions of this investigation. Variations in base pressure coefficient as a function of Mach number for blunt-base models of 0.50 percent and 3.25 percent tunnel blockage ratio are compared with free-flight data.


## NOMENCLATURE

| | |
|---|---|
| $C_{p,b}$ | Base pressure coefficient, $(p_b - p_\infty)/q_\infty$ |
| $C_{p,b_\ell}$ | Base pressure coefficient based on flow conditions at the model base as determined from a static pressure centerline probe, $(p_b - p_\ell)/q_\ell$ |
| $M_\infty$ | Free-stream Mach number |
| $M_\ell$ | Mach number based on flow conditions at a specific tunnel station derived from $(p_\ell/p_t)$ |
| $p_b$ | Average base pressure, psf |
| $p_c$ | Plenum chamber static pressure, psf |
| $p_d$ | Static wall pressure measured at tunnel station 36.00, psf |
| $p_\ell$ | Local static pressure measured on a centerline static pressure probe, psf |
| $p_t$ | Stilling chamber total pressure, psf |
| $p_t'$ | Diffuser exit static pressure, psf |
| $p_\infty$ | Mean free-stream static pressure measured on the centerline probe ahead of test section station 25.0, psf |
| $q_\infty$ | Free-stream dynamic pressure, $0.7\ p_\infty M_\infty^2$, psf |
| $q_\ell$ | Local dynamic pressure $\left(0.7\ p_\ell M_\ell^2\right)$, at a specific tunnel station derived from $(p_\ell/p_t)$, psf |
| $T_t$ | Stilling chamber total temperature, °F |
| u | Velocity of flow parallel to the tunnel centerline at a distance y from the model support tube, ft/sec |

| | |
|---|---|
| $V_\infty$ | Free-stream velocity, ft/sec |
| $y$ | Distance measured perpendicular from the model support tube, in. |
| $\delta$ | Boundary layer thickness, in. |
| $\lambda$ | Tunnel pressure ratio, $p_t/p_t'$ |

## INTRODUCTION

Consistent base pressure measurements have been difficult to obtain when models have been installed in the aft part of a transonic wind-tunnel test section. This problem is of particular concern when full-scale propulsion units are tested. These test installations — consisting of inlet ducting, engine, exit nozzle, and structural frame-work — naturally require a greater utilization of the test section length than is required for aerodynamic tests.

Since large test installations are often tested in the Propulsion Wind Tunnel at AEDC, an investigation of the problem was made. The 1-Ft Transonic Tunnel (described in Ref. 1) was used for the tests. Although the absolute values of the governing parameter (tunnel pressure ratio) apply only to the 1-ft tunnel, the trends indicated should be applicable to any tunnel with partially open walls.

Data obtained from other tests in the 1-ft tunnel indicate that the Mach number distribution in the aft section of the test section can be drastically affected by variations in tunnel pressure ratio (Ref. 2). Thus changes in tunnel pressure ratio were expected to affect base pressure measurements, and this investigation was directed toward obtaining consistent base pressures with tunnel pressure ratio ($\lambda$) as the varying parameter. A particular effort was made to determine the exact pressure ratio required to obtain consistent pressure measurements with the model base located at various tunnel test section stations.

## APPARATUS

### 1-FT TRANSONIC TUNNEL

The investigation was conducted in the 1-Ft Transonic Tunnel (Ref. 1), which is a continuous-flow, open-circuit tunnel (Fig. 1). The test section is comprised of four perforated walls forming a working section 12 by 12 in. in cross section and 37.5 in. in length. A sketch of the wall liners and a schematic layout of the test section are shown in Fig. 2.

The total pressure in the tunnel is kept constant at approximately 1.4 atmospheres, and variable density operation is not possible. The tunnel total temperature ($T_t$) may be varied to avoid condensation by recirculating

Manuscript released by author November 1958.

some of the inlet airflow. The total temperature can be varied from approximately 140° F at a Mach number of 0.70 to 210° F at a Mach number of 1.4 depending on the atmospheric conditions at the compressor inlet.

## TEST ARTICLES

The basic test articles are shown in Figs. 3 through 6. The infinite-length body (see Figs. 3 and 4) consists of a 2.44-in. O.D. pipe extending from the stilling chamber into the test section. Additional lengths of pipe could be added to position the afterbodies (A or B) at four test section stations. The porous section in the pipe, shown in Fig. 4, was used to investigate the effects of boundary layer removal on base pressure. A 1.0-in.-diam pipe similar to model A was tested to determine base pressures that were considered to be free from wall interference. The wall support structure used with the infinite-length body is shown in Fig. 3. Also shown in Fig. 3 are the locations of the orifices from which the base pressures were obtained and averaged to determine the base pressure coefficients. The finite-length body (see Figs. 5 and 6) is composed of a 25° 20' conical forebody, a 2.44-in. O.D. cylindrical center section and either the blunt-base (A) or boattail (B) afterbody. The sidewall struts were not identical for the finite- and infinite-length bodies. The thickness ratio was approximately equal for both struts (0.0650), but the finite-length body strut was larger because of structural requirements.

## PRECISION

The estimated precision of measurements made during the tests is given in the following table:

| | $M_\infty = 0.70$ | $M_\infty = 1.30$ |
|---|---|---|
| $C_{p,b}$ | ±0.008 | ±0.008 |
| $M_\infty$ | ±0.010 | ±0.020 |
| $\lambda$ | ±0.008 | ±0.005 |

The inaccuracies for Mach number quoted above are for variations in the vicinity of the test article positioned at station 21.90 as determined from the tunnel empty centerline distributions. The inaccuracies in setting Mach number are ±0.005 and ±0.003 for Mach number 0.70 and 1.30, respectively.

## RESULTS AND DISCUSSION

Several factors were considered in the choice of the primary test article configuration for the investigation. The infinite-length body was chosen in preference to the finite-length body mainly because the bow shock waves would not be present on an infinite-length body and therefore would not introduce another parameter into the experiment. Also it was more convenient to position the model base at different test section locations. With the infinite-length body there was the possibility of affecting the base pressures caused by the additional boundary layer build-up with increases in body length; however, an investigation of the effect of lengthening the body on base pressure (discussed later) revealed that the effects were negligible.

The longitudinal variations of static pressure within the test section with changes in tunnel pressure ratio, $\lambda$, are shown in Fig. 7 for Mach numbers 0.70, 0.90, 1.10, and 1.30. The region in which the static pressure deviates from free-stream conditions primarily as a function of the tunnel pressure ratio is confined to the rearward portion of the test section. At subsonic Mach numbers, decreasing pressure ratio causes a decrease in Mach number which moves forward along a line from the rear of the test section. Tunnel pressure ratio can be decreased to the point where the airflow through the walls is at a maximum (full plenum capacity) and where any further decrease will reduce the free-stream Mach number throughout the test section. As the pressure ratio is increased beyond an optimum value, an increase in Mach number results in the rear of the test section until the Mach number level can no longer be maintained (auxiliary plenum removal equal to zero) (see Fig. 7a) or the diffuser entrace is choked (see Fig. 7b). Once the diffuser entrace is choked an increase in pressure ratio serves only to accelerate the flow in the diffuser. At supersonic Mach numbers (Figs. 7c and 7d) insufficient pressure ratio causes a shock wave system forward of the diffuser entrace in the rearmost portion of the test section. As pressure ratio is increased, the shock wave system moves into the diffuser. Beyond an optimum value (i.e., $\lambda = 1.32$ at $M = 1.30$), an increase in tunnel pressure ratio accelerates the flow in the diffuser as in the subsonic case.

### BLUNT-BASE INFINITE-LENGTH MODEL A

The tunnel pressure ratio required to obtain a consistent base pressure measurement was determined with the base of the test article at four longitudinal tunnel stations ranging from station 21.80 to 36.16. At each tunnel station the variation of $C_{p,b}$ as a function of $\lambda$ was obtained throughout the Mach number range. These variations are presented in Fig. 8 for Mach numbers 0.70, 0.90, 1.10, and 1.30. Results from an

interpolation of similar data show the variation of $C_{p,b}$ with changes in model base location for particular values of $\lambda$ (Fig 9). A comparison of Figs. 8 and 9 with Fig. 7 indicates the criteria for the proper positioning of the test article within the test section. At subsonic Mach numbers, the desired $C_{p,b}$ can be obtained throughout the test section if the static pressures from the tunnel empty centerline indicate that the free-stream Mach number extends about 1.5 base diameters beyond the model base. Figure 7a shows that when the model base is positioned at station 36.16 only a single value of $\lambda$ will extend the free-stream Mach number 1.5 base diameters aft of the model. The model base pressure is influenced by either the decrease in pressure (increasing $\lambda$) or the increase in pressure (decreasing $\lambda$) in the rearward portion of the test section. Note that at Mach number 0.70 with the model base at station 21.80 (see Fig. 8a) only an increase in pressure is shown in the $C_{p,b}$, indicating that the point within the test section at which the flow is accelerated with increasing $\lambda$ is far enough downstream not to influence the base pressure; therefore, the base pressure levels off to a value assumed to be optimum. Naturally, as the model base is moved aft a point is reached where the influence of the accelerating flow and the resulting compression shock wave system in the diffuser is reflected in the base pressure — for example, see data shown in Fig. 8b at Mach number 0.90 with the model base positioned at station 33.14. At values of $\lambda$ less than 1.25, the base pressure is influenced by the expansion into the 7-deg conical diffuser and by the terminating compression system. At $\lambda$ values greater than 1.25, the compression system has moved downstream far enough not to influence the base pressure; therefore, only the influence of the expansion is left. As $\lambda$ is increased, the initial Mach wave emanating from the junction of the test section exit and diffuser entrance remains fixed while the downstream extent of the expansion region is a function of $\lambda$ (progressing downstream as $\lambda$ increases until the tunnel pressure ratio can no longer sustain the flow). When the model is moved aft (36.16), higher values of $\lambda$ are required to obtain a plateau on the curve (Fig. 8b) since the compression system is closer initially. The closer the model base is positioned to the expansion and compression regions, the greater the influence on base pressure as evidenced by Fig. 8b.

At supersonic Mach numbers essentially the same flow phenomena occurs as at the high subsonic Mach numbers. Figures 7c and 7d show that the free-stream Mach number extends further downstream as the Mach number increases as a result of the inclination of the expansion region. Obviously, the terminating compression system also moves aft with increasing Mach number. As shown in Fig. 8c with the model placed between stations 29.8 and 33.14, only the compression system affects the base pressure. At station 36.16 the expansion and compression for values of $\lambda$ below 1.25 influenced the base pressure. Values of $\lambda$ greater than 1.25 reflect only the influence of the expansion. At Mach number 1.30 (see Fig. 8d) the only influence shown in the $C_{p,b}$ is that from the compression region in the diffuser, which indicates that the expansion region

is not impinging on the model wake and thus influencing the base pressures. This is possible since the initial Mach wave of the Prandtl-Meyer expansion intersects the tunnel centerline approximately 2.6 base diameters aft of the model. The data indicate that disturbances are being propagated upstream through the subsonic wake of the model from the compression system. At station 36.16 (Fig. 8d) the desired base pressures can only be obtained with maximum $\lambda$ which positions the compression shock wave system as far downstream as possible. At least three base diameters of constant pressure beyond the model are required for a supersonic Mach number to obtain desired base pressures.

The range of $\lambda$ required to obtain the desired base pressure for model A is presented in Fig. 10. As the model is moved aft in the test section, the range of $\lambda$ that will produce the desired base pressures decreases. Placing the model beyond station 29.8 and operating at a Mach number above sonic velocity where only one value of $\lambda$ will produce the desired base pressure should be avoided. During such operation the base pressure is in a balanced state where the effects of the expansion are off-set by the compression region downstream of the model. If operation at this condition is required, a thorough calibration of the wind tunnel with the test model within the test section must be conducted to determine the correct value of $\lambda$. At low subsonic Mach numbers the centerline distribution from the empty tunnel will adequately indicate the correct $\lambda$ for tunnel operation.

A crossplot of the base pressure coefficients obtained at the correct $\lambda$ values for model A versus test section Mach number is presented in Fig. 11. Also shown are free-flight data from Refs. 3 and 4 and data obtained from the 1.00-in. diam Model A. The base of the 1.00-in.-diam body was positioned at the 20-in. tunnel station to avoid $\lambda$ effects. The agreement between the free-flight data of Ref. 4 and the data from the 0.5 percent (1.00-in.-diam) blockage model is fairly good. The free-flight data from Ref. 3, however, shows a more rapid decrease in base pressure with increasing Mach number than does the other data. Correlation between the large and small models (A) is poor at Mach number 0.70 and not very good at 1.0 and 1.40. The base pressure decrease is delayed at Mach number 1.0 for the larger model. This result is in qualitative agreement with Ref. 5, which indicates a delay in base pressure decrease at Mach number 1.0 as model blockage is increased. No mention of $\lambda$ effects is made in Ref. 5; therefore, the large blockage effects shown in that reference may be a combined result of $\lambda$ and blockage ratio effects.

Slight variations in $\lambda$ can greatly affect base pressure measurements with the model positioned aft in the test section as shown in Fig. 8. The values of $C_{p,b}$ shown there are based on free-stream conditions ($V_\infty$, $p_\infty$, $q_\infty$) and are not indicative of the variation of $C_{p,b}$ with respect to the local

Mach number at the model base because the variations in $\lambda$ have changed the flow conditions at the model base. The two parameters in base pressure measurements are the Mach number changes at the model base and the Mach number gradient on the model wake. To determine which parameter is of prime importance, the change in local Mach number at the model base and the $C_{p,b}$ based on local flow conditions must be determined. See, for example, the data obtained at tunnel stations 33.14 and 33.16.

At tunnel station 33.14, the Mach number corresponding to the local values of $p_\ell/p_t$ from Fig. 7a was determined for various values of $\lambda$; also, $C_{p,b}$ data from Fig. 8a were recomputed using the local stream conditions at station 33.14. Both parameters $M_\ell$ and $C_{p,b_\ell}$ are presented in Figs. 12 and 13 as a function of $\lambda$. If $C_{p,b}$ were solely a function of the Mach number at the model base, the change in $C_{p,b}$ shown in Fig. 13 would correspond to the change expected from a variation in Mach number from 0.688 to 0.768. Results obtained from prior model A tests indicate that the change in $C_{p,b}$ should be about 0.025 for this change in Mach number. As shown in Fig. 14, the change in $C_{p,b_\ell}$ is approximately 0.22 or 8.8 times greater than would be expected from a change in free-stream Mach number over the model.

The effects of a pressure gradient on the model wake are further illustrated when the model base is positioned at station 36.16. The local Mach number and base pressure coefficients were calculated in the same manner as discussed in the preceding paragraph and are also presented in Figs. 12 and 13. Again, the change in $C_{p,b_\ell}$ is 4.4 times greater than would be expected from a variation in Mach number from 0.663 to 0.832 (Fig. 12). The rate of change in $M_\ell$ with variations in $\lambda$ is greater at stations 36.16 and 33.14, and the change in $C_{p,b_\ell}$ at the model base is less at stations 36.16 and 33.14. Apparently the Mach number change at the model base is a minor factor in affecting base pressure measurements, and the Mach number (static pressure) gradient over the model wake is the prime parameter.

In an attempt to arrive at a visual indicator which would show the proper pressure ratio setting while the tunnel is in operation, a method was tried wherein an average static pressure at the test section exit was employed. The exit static pressure ($p_d$) was measured circumferentially on the tunnel walls at station 36.00. Plenum pressure ($p_c$) is indicative of the average free-stream static pressure, $p_\infty$, with $p_c$ being slightly greater. When the ratio of $p_d$ to $p_c$ approaches 0.975 (see Fig. 15a), the test section at station 36.00 is essentially at free-stream conditions. For subsonic Mach numbers (see Figs. 15a and 15b) the correct base pressure can be obtained when the ratio of $p_d$ to $p_c$ approaches 0.975. It should be

noted, however, that the desired base pressure measurement can be obtained over a wide range of $p_d/p_c$ when the model is located appreciably forward of the measuring station (36.00). Figures 15a and 15b show that for subsonic operation $p_d$ can be used as an indicator in setting the correct $\lambda$.

At supersonic Mach numbers (see Figs. 15c and 15d) the 0.975 setting of $p_d$ to $p_c$ yields the desired base pressure readings only for the two forward model base locations. The influence of the expansion region which emanates from the model base on $p_d$ is clearly shown in Fig. 15c when the model is placed at station 33.14. With the model base located at stations 33.14 and 36.16, the ratio of $p_d$ to $p_c$ remains essentially constant over wide variations in $C_{p,b}$. This indicates that the rearward portion of the test section at the wall is at the free-stream Mach number but that the expansion and compression regions at the test section exit and diffuser entrace are influencing the base pressures as explained in an earlier paragraph. At Mach number 1.30 (Fig. 15d) the ratio $p_d/p_c$ indicates free-stream conditions for the two aft model locations, but the desired base pressure is not obtained for any value of $\lambda$ less than maximum. At Mach number 1.30 only the effects of the compression shock wave system are reflected in the data. For supersonic operation the ratio $p_d/p_c$ is not an adequate indicator unless the measuring orifices ($p_d$) are at least 2.5 base diameters downstream of the model, which is not possible for models placed in the rearmost portion of the test section. The orifices ($p_d$) must be carefully located to avoid shock wave reflections from the model.

One parameter not discussed in the preceding sections is the possible variation in base pressure with regard to changes in model length. The ratio of boundary layer thickness at the model base to the base diameter is a factor in determining base pressure. Thus as model length was increased the boundary layer thickness was proportionately increased. A porous section was installed in the infinite length body (see Fig. 4) as a means of boundary layer removal to obtain the effect of boundary layer thickness, $\delta$, on base pressure. The investigation, although limited, revealed that the displacement thickness of the boundary layer could be reduced by a factor of two and not reflect changes in base pressure. Since the change in $\delta$ with model length was within this range of variation, the changes in body length made during this program did not affect the base pressure measurements. This conclusion was anticipated since the change in $\delta$ varies inversely as the one-fifth power of Reynolds number (Refs. 6 and 7) for turbulent boundary layers (see Fig. 16). Therefore $C_{p,b}$ should be insensitive to changes in model length for the Reynolds number range of this investigation.

## BOATTAIL INFINITE-LENGTH MODEL B

The changes in $C_{p,b}$ with test section station at constant values of $\lambda$, presented in Fig. 17, were derived in the same manner as those for model A. As shown in Fig. 17, the trends are not as decisive for model B as those for model A. Also, a smaller change in $C_{p,b}$ was obtained with model B than with model A for a comparable change in $\lambda$ (see Figs. 9a and 17a). Model B has a smaller wake, thus enabling the low momentum air in the wake to be transferred to the free stream in a shorter distance downstream of the base. The closer the wake dissipates to the model base, the less the pressure gradients downstream can affect the base pressure measurements. In the majority of cases, values of $\lambda$ less than a maximum can be used to produce the desired base pressures for the supersonic test Mach numbers and indicate that disturbances emanating from the diffuser shock system are also minimized for models with small wakes. In essence, the model wake has dissipated before reaching the diffuser shock system; thus disturbances from the diffuser are not propagated upstream through the subsonic model wake. Reasons for the peculiar trends in the curves with the model base in the vicinity of station 29.8 are not known.

## FINITE-LENGTH MODELS A AND B

Base pressure coefficients as a function of $\lambda$ for the finite-length models A and B are presented in Figs. 18 and 19. These configurations were investigated primarily to gain an insight into the effects of $\lambda$ on base pressures for more realistic model configurations and to determine whether base pressure variations with changes in $\lambda$ were similar for the infinite- and finite-length bodies. Both configurations were tested at one longitudinal tunnel station (29.73), and therefore a correct operating $\lambda$ was not established. However, at supersonic Mach numbers, $\lambda$ effects are insignificant at this base station. Comparing the data for the finite- and infinite- length models (see Figs. 18 and 19) throughout the Mach number range at a comparable $\lambda$ reveals that, although the base pressures are consistently lower for the finite-length body, the trends in the data are nearly duplicated. Three obvious factors enter into the discrepancy in the level of the base pressures; the ratio of boundary layer thickness to base diameter, model nose configuration, and the ratio of support strut wake to base diameter, the support strut being much larger for the finite-length model because of structural requirements. However, since the trends in the curves are similar, the conclusions drawn from the infinite-length body results may apply equally as well to the finite-length models.

## CONCLUSIONS

This investigation of base pressure effects resulting from changes in tunnel pressure ratio resulted in the following conclusions:

1. The tunnel pressure ratio required for subsonic tunnel operation can be defined rather accurately from the tunnel empty pressure distributions if the value that extends the free-stream Mach number as far downstream as possible is chosen.
2. For supersonic operation a balancing effect between the expansion fan and diffuser terminal shock system complicates the problem of defining the correct pressure ratio when the model is placed in the aft portion of the test region. By positioning the model sufficiently forward of the diffuser entrance this balancing effect can be avoided.
3. Static pressure orifices placed in the rearward portion of the test section will indicate the proper tunnel pressure ratio for subsonic operation. For supersonic operation, the static orifices must be placed at least 2.5 base diameters downstream of the model base for proper indication.
4. The predominate factor influencing base pressure measurements is the static pressure gradient on the model wake resulting from changes in tunnel pressure ratio.
5. The conclusions presented for the infinite-length body apply equally as well to the finite-length body since the effects of tunnel pressure ratio on base pressure are similar.

## REFERENCES

1. Test Facilities Handbook. "Propulsion Wind Tunnel Facility, Volume III." Arnold Engineering Development Center, January 1958.
2. Goethert, B. H. "Influence of Plenum-Chamber Suction and Wall Convergence on Mach Number Distributions in Partially Open Test Sections of Wind Tunnels at Subsonic and Supersonic Speeds." AEDC-TR-54-42, April 1955.
3. Peck, Robert F. "Flight Measurements of Base Pressure on Bodies of Revolution with and without Simulated Rocket Chambers." NACA TN 3372, April 1955.
4. Hart, Roger C. "Effects of Stabilizing Fins and a Rear-Support Sting on Base Pressures of a Body of Revolution in Free Flight at Mach Number 0.70 to 1.3." NACA RM L52E06, September 1952.

5. Pel, C. and Rustemeyer, A. "Investigation of Turbojet Exhaust Interference Drag." UAC R-0801-12, November 1955.

6. Chapman, Dean R. "An Analysis of Base Pressure on Supersonic Velocities and Comparison with Experiment." WADC TN 2137, July 1950.

7. Raymond, J. L. and Rodden, W. P. "Base Pressures for Bodies of Revolution." Rand Corporation, RM-1544, August 1955. (Confidential)

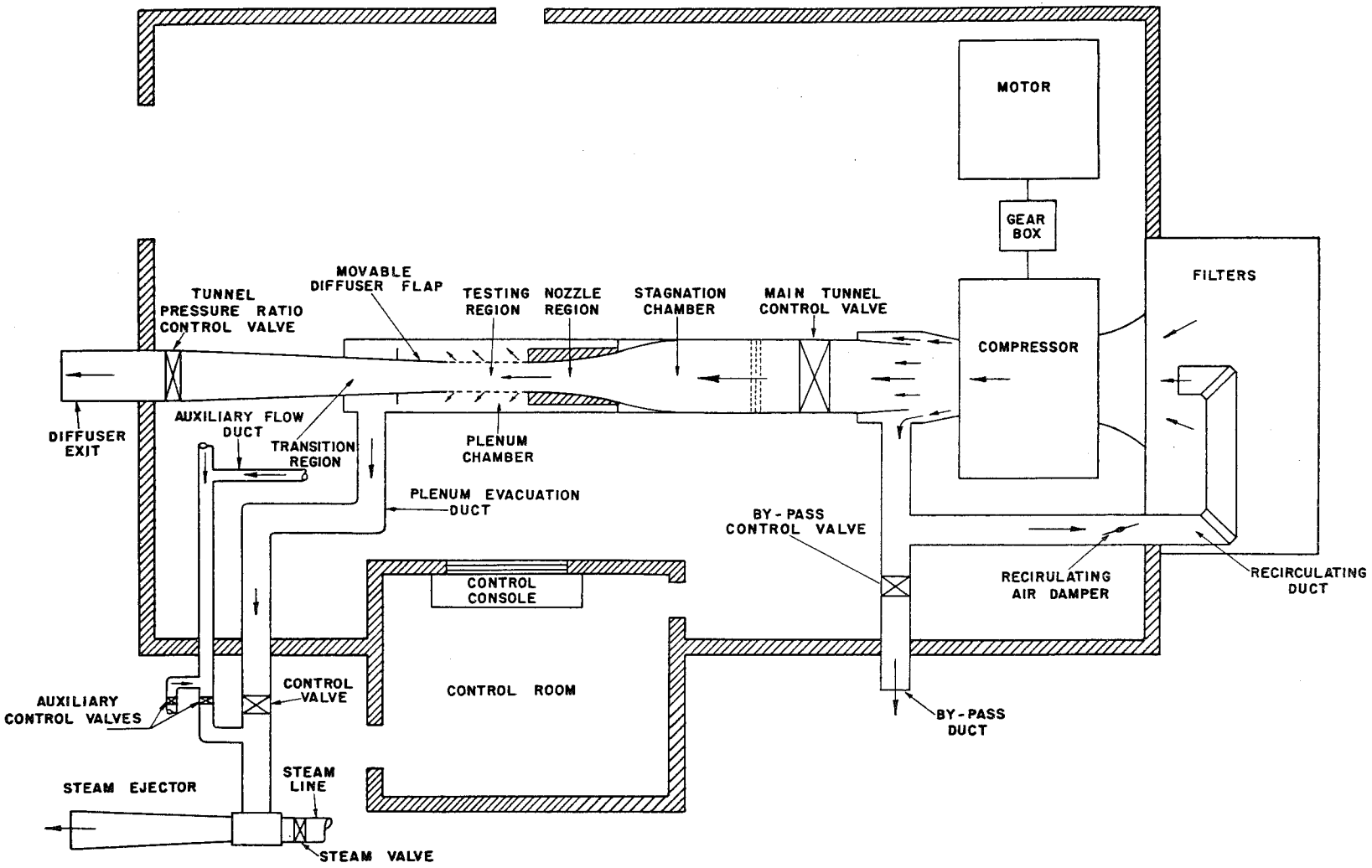


Fig. 1. General Arrangement ot the 1-Ft Transonic Tunnel and Supporting equipment

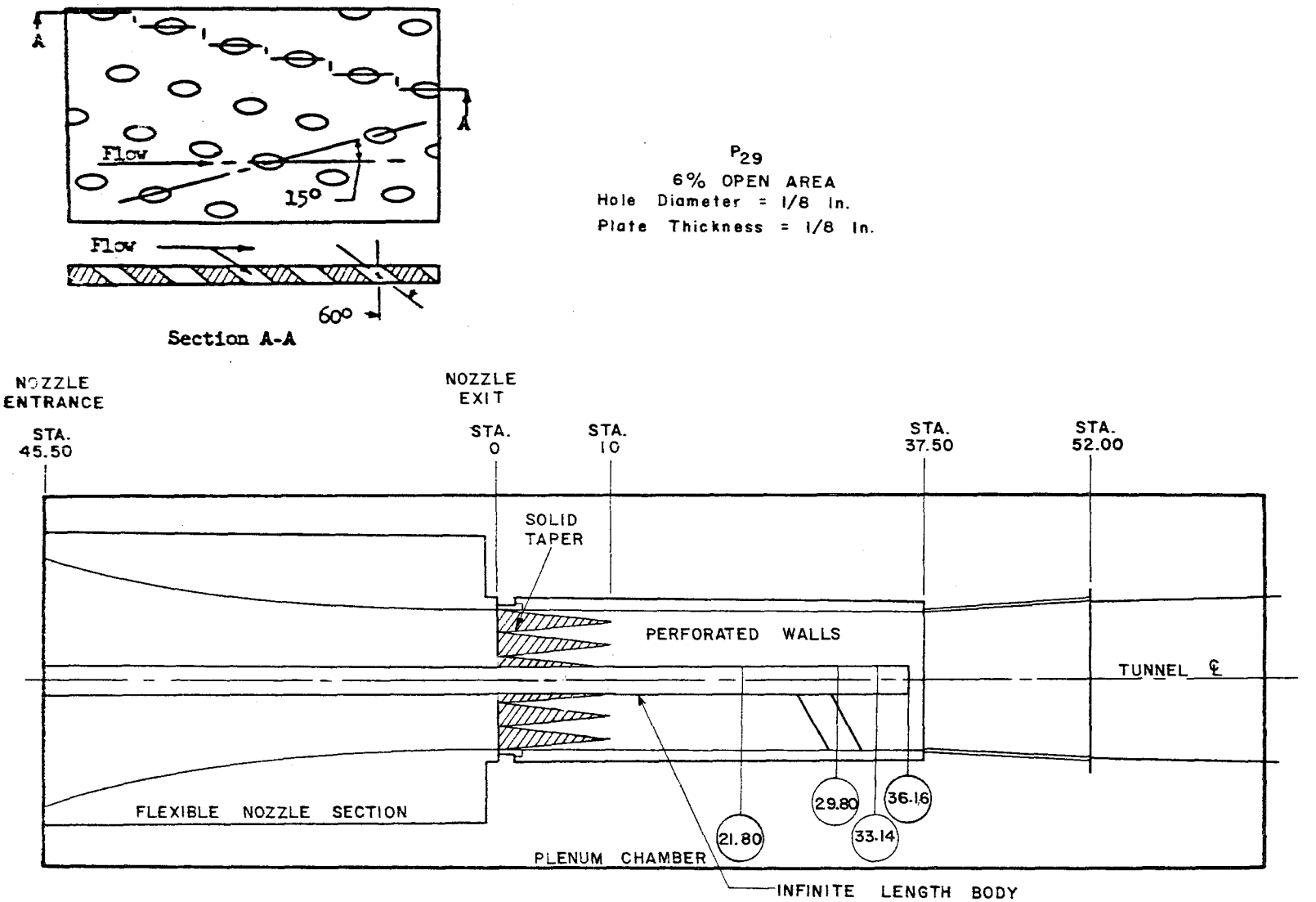


Fig. 2. Schematic of the 1-Ft Transonic Tunnel and Wall Liners with the Infinite-Length Body

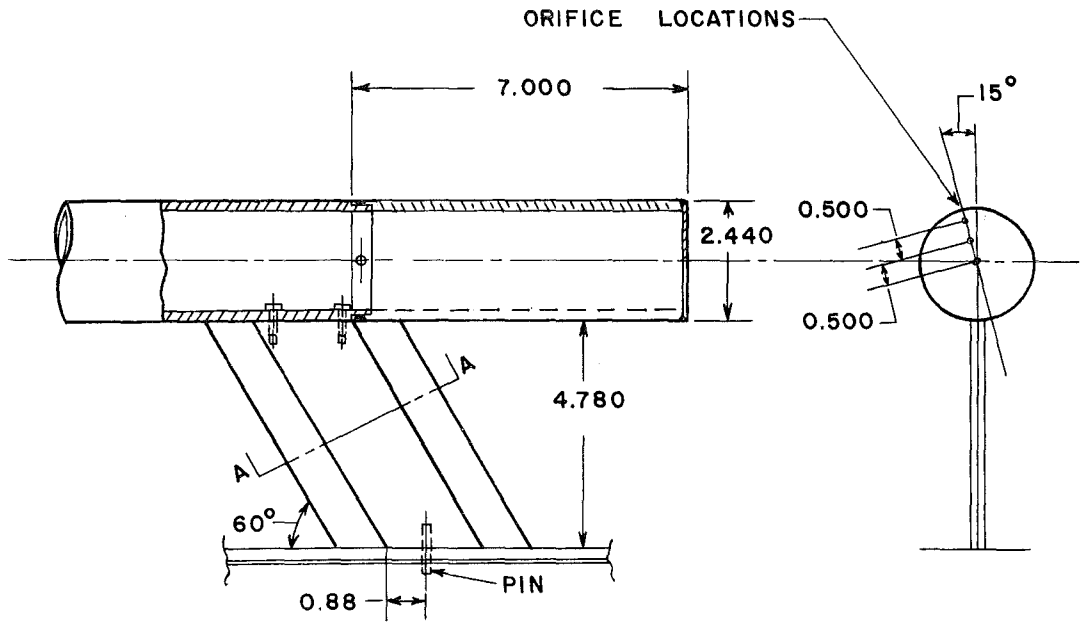


a. Blunt-Base Model A

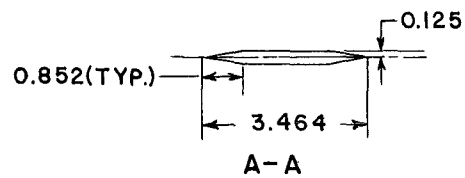


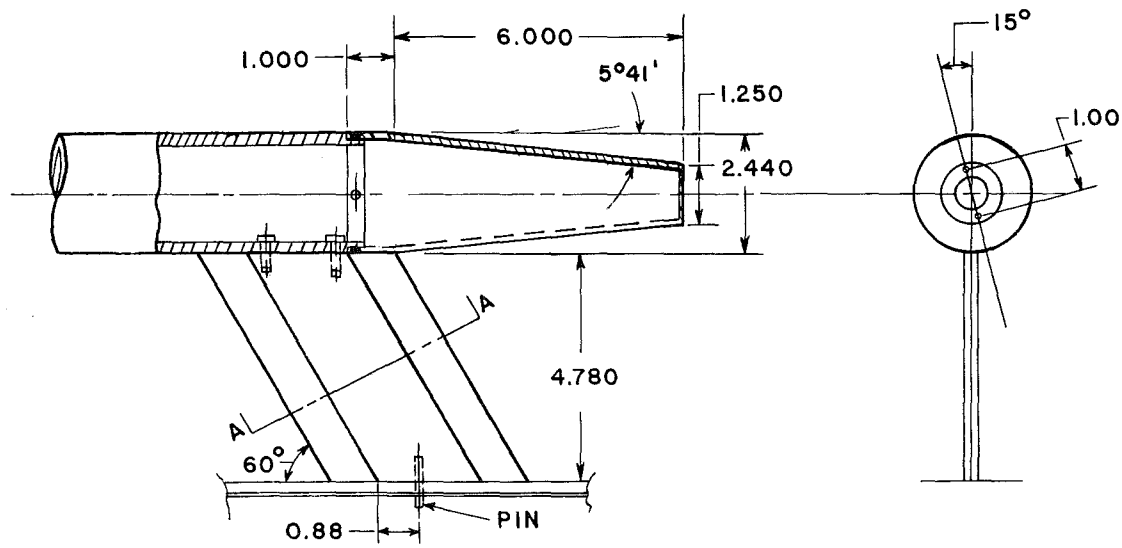


NOTE: ALL DIMENSIONS IN INCHES

b. Boattail Model B

Fig. 3. Details of the Infinite-Length Model with After-bodies A and B

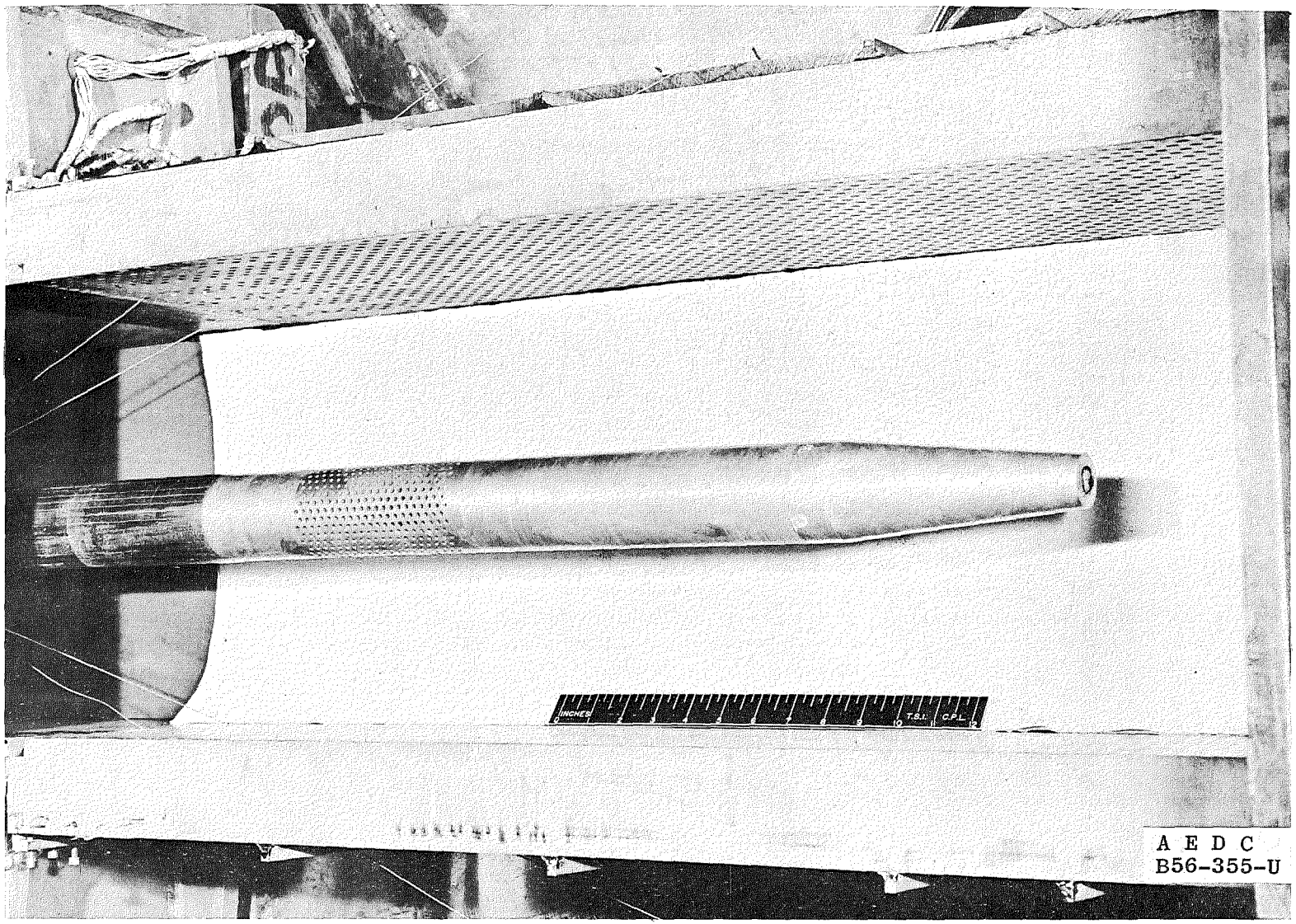


Fig. 4. Infinite-Length Model B Installed in the 1-Ft Transonic Tunnel Test Section

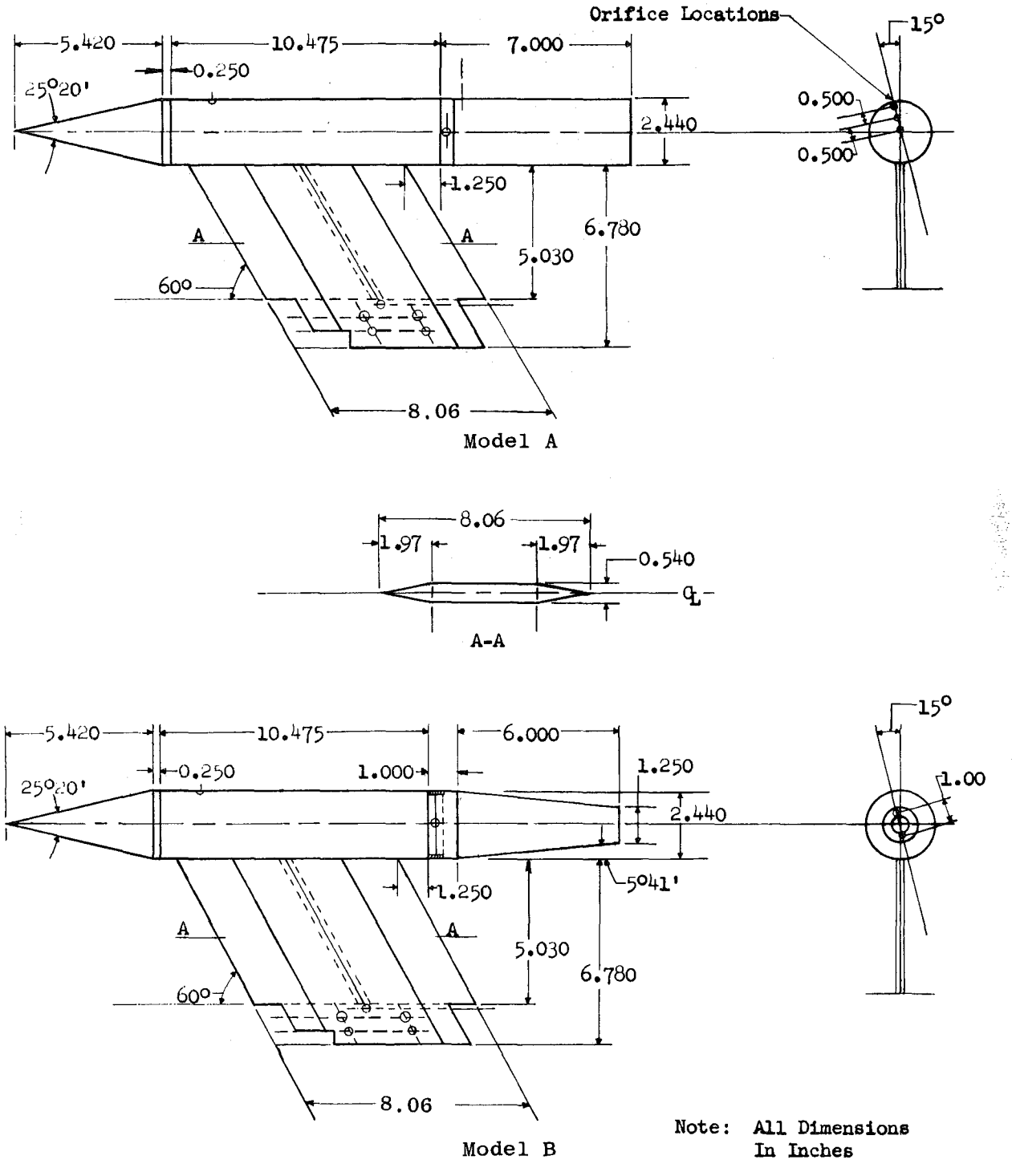


**Fig. 5. Details of Finite-Length Models A and B**

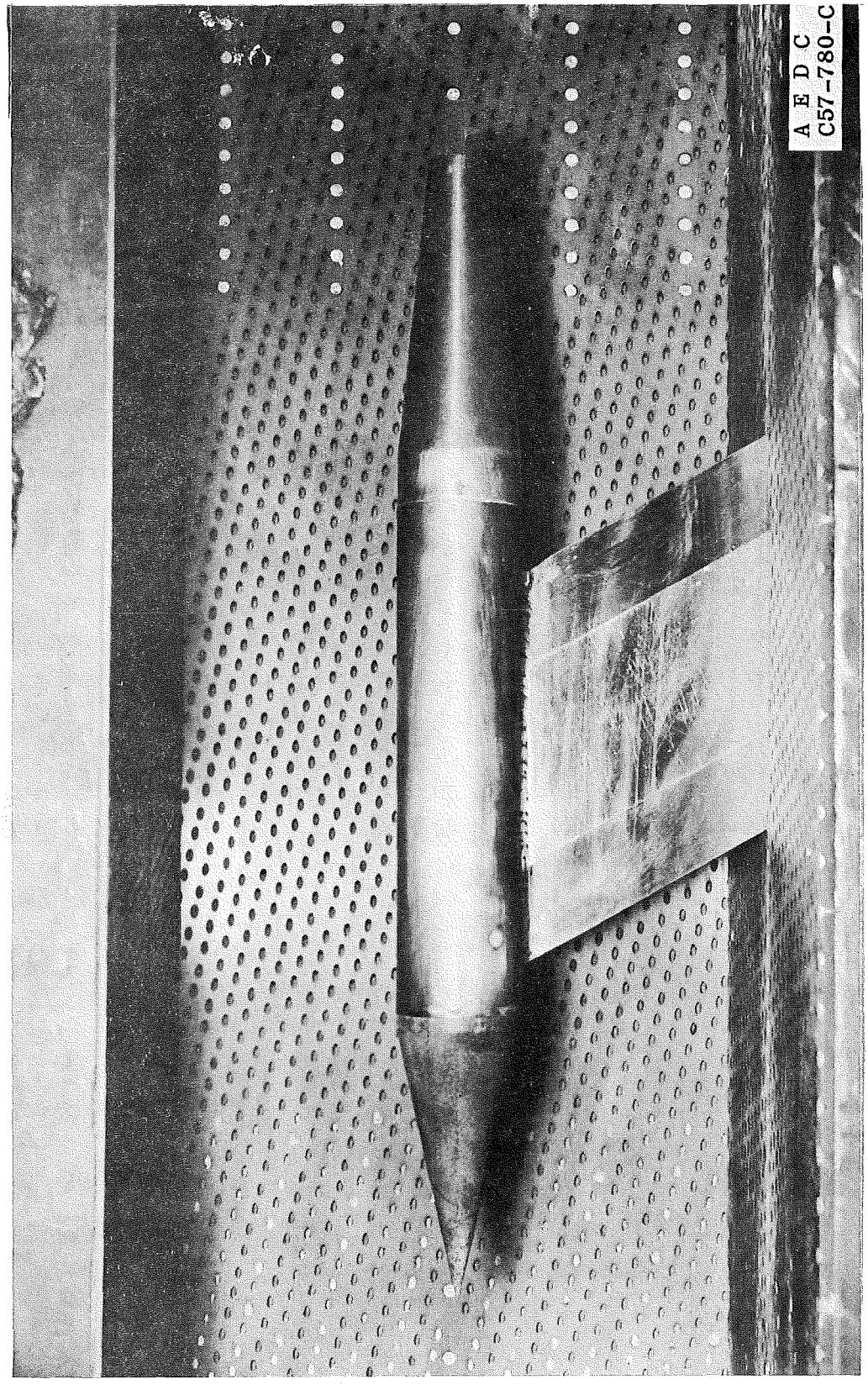


Fig. 6. Finite-Length Model B Installed in the 1-Ft Transonic Tunnel Test Section

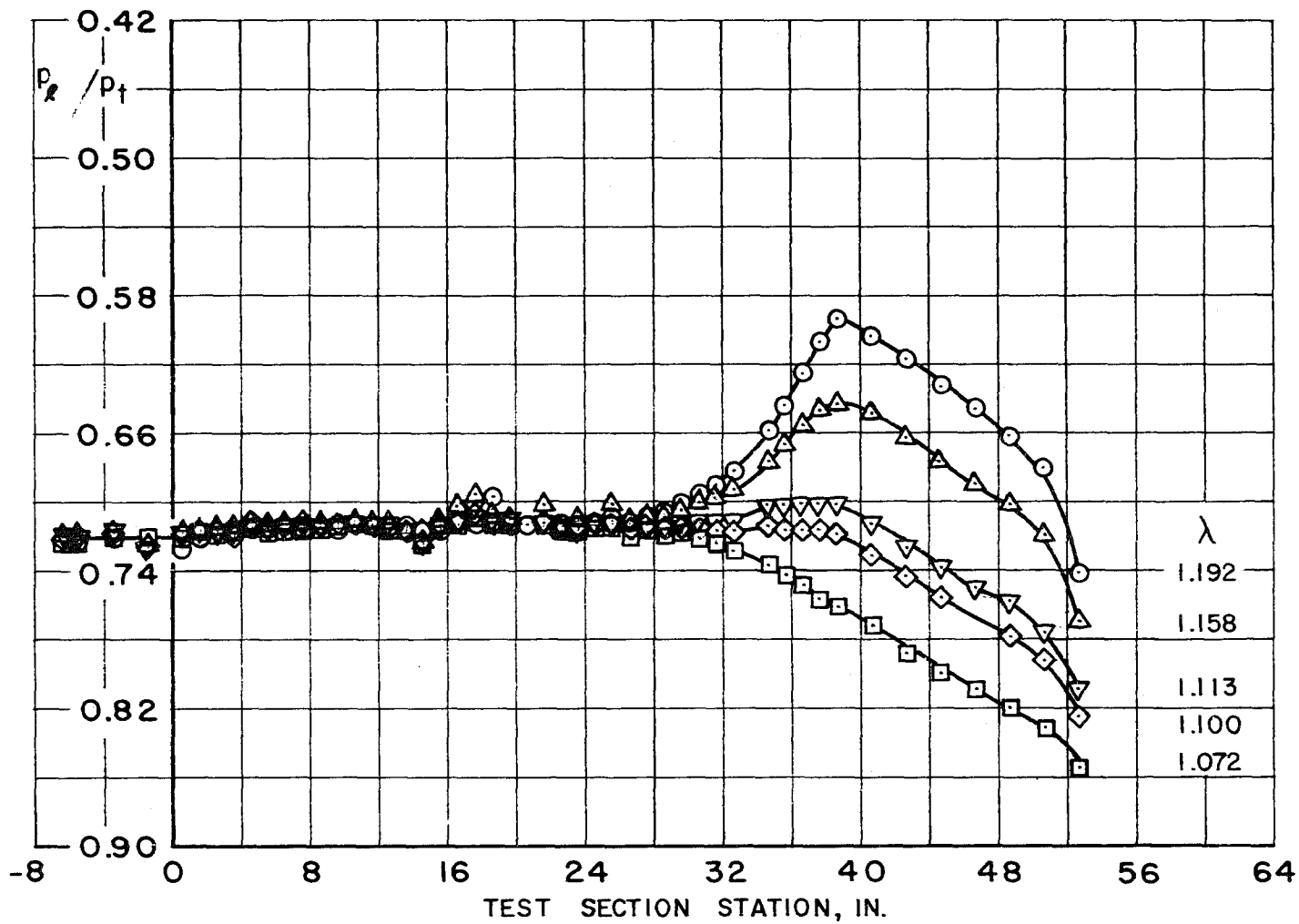


a. Mach Number 0.70

Fig. 7. Test Section Centerline Static Pressure Distributions

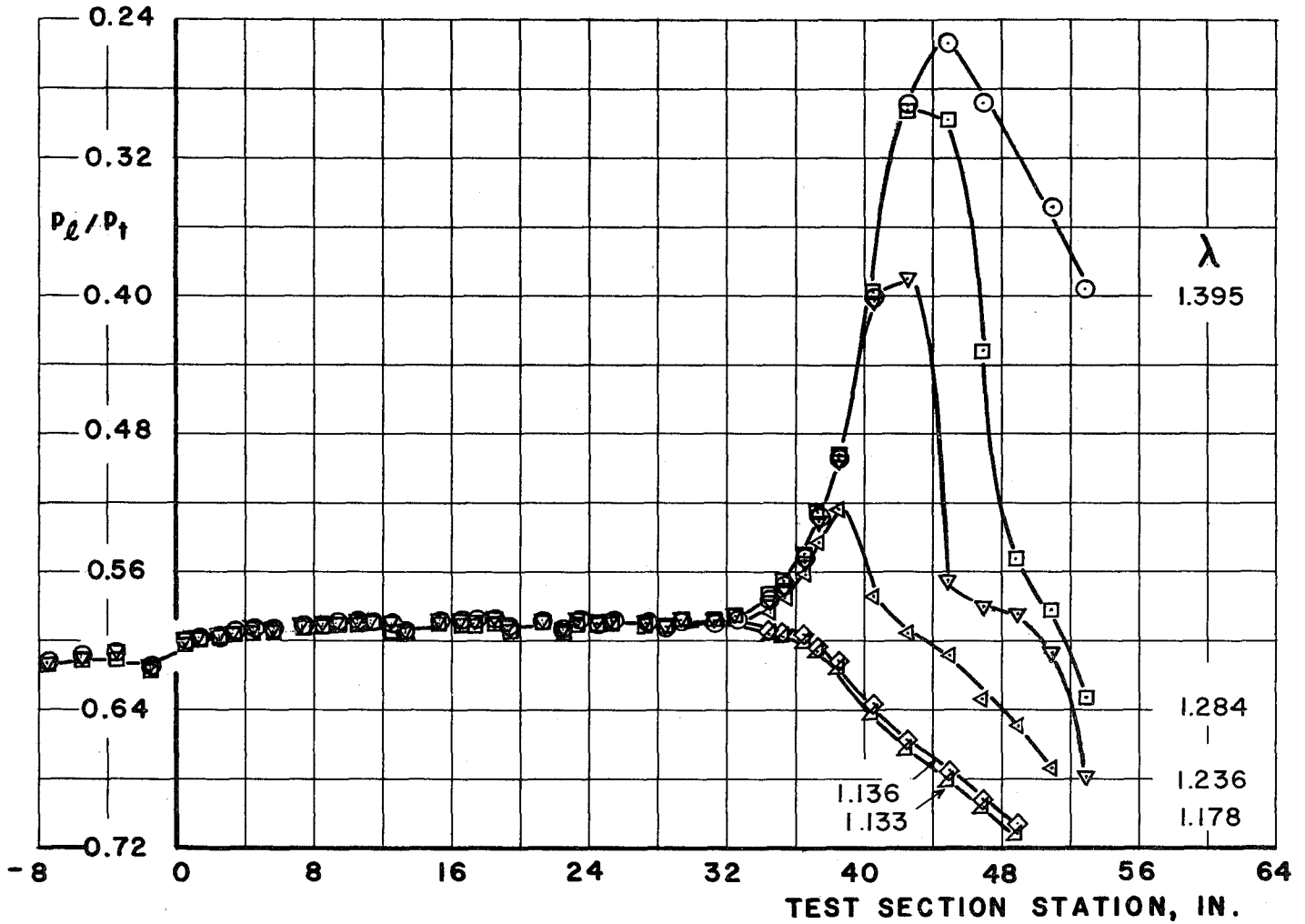


b. Mach Number 0.90

Fig. 7. Continued

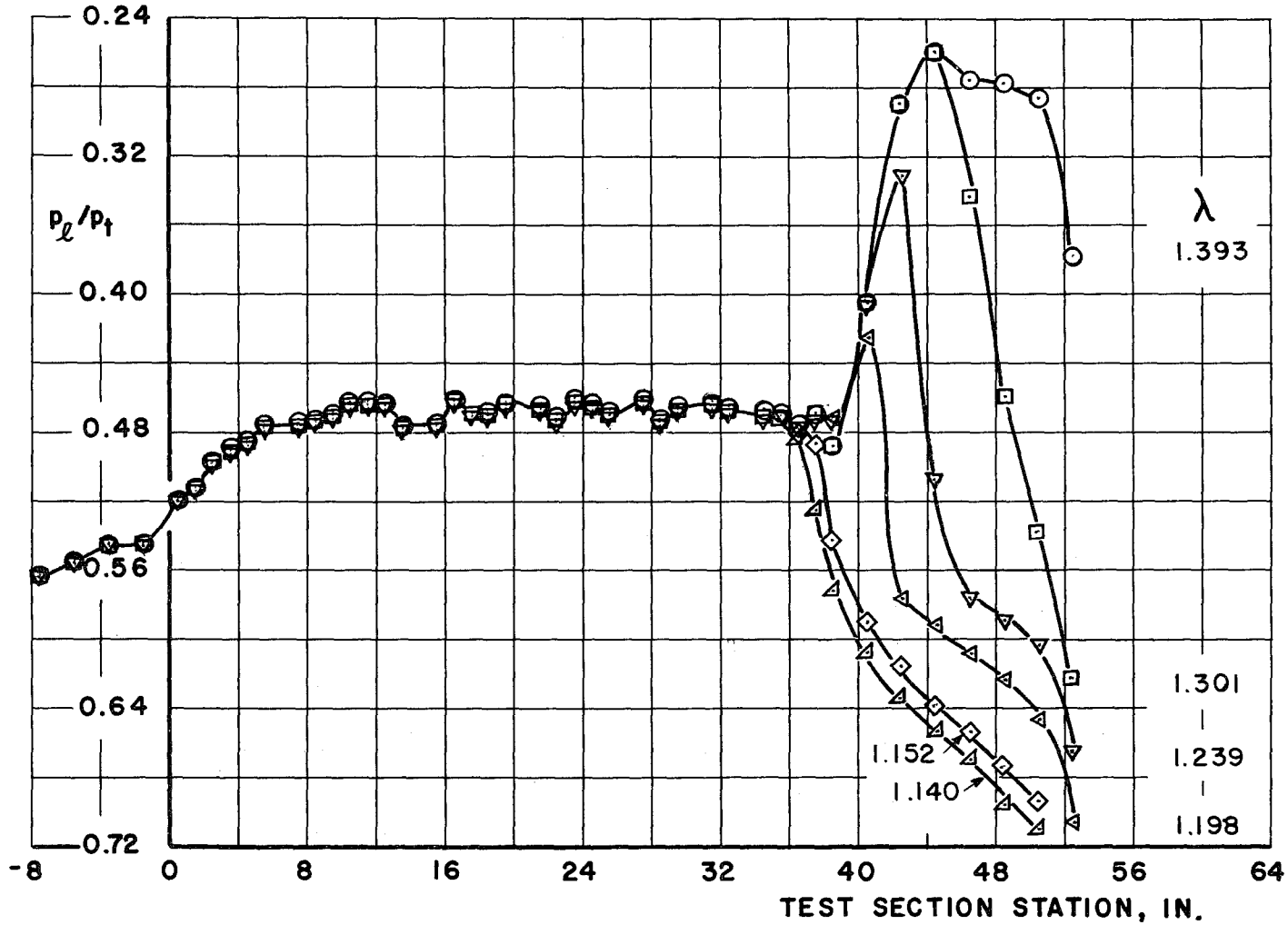


c. Mach Number 1.10

Fig. 7. Continued

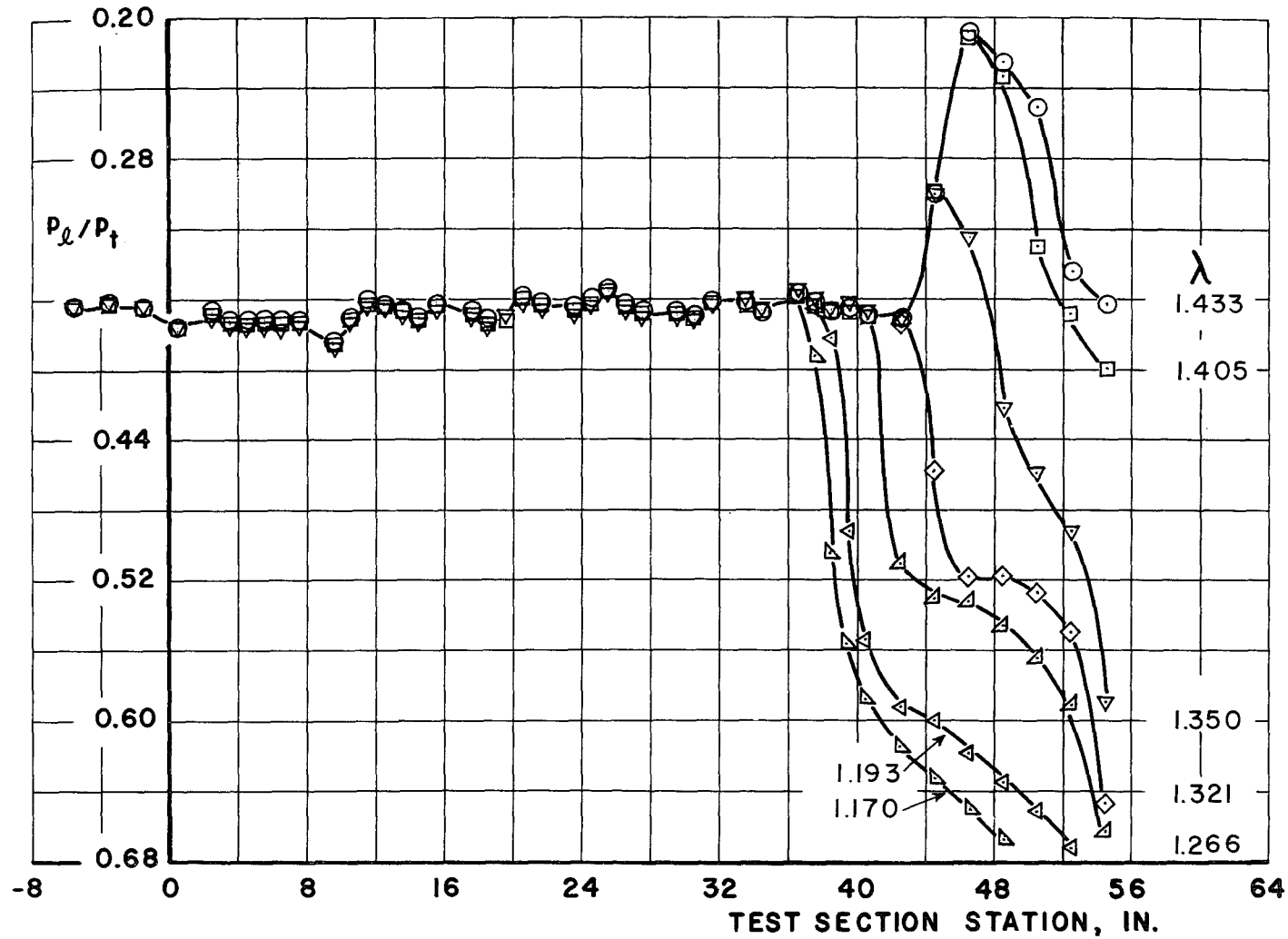


d. Mach Number 1.30

Fig. 7. Concluded

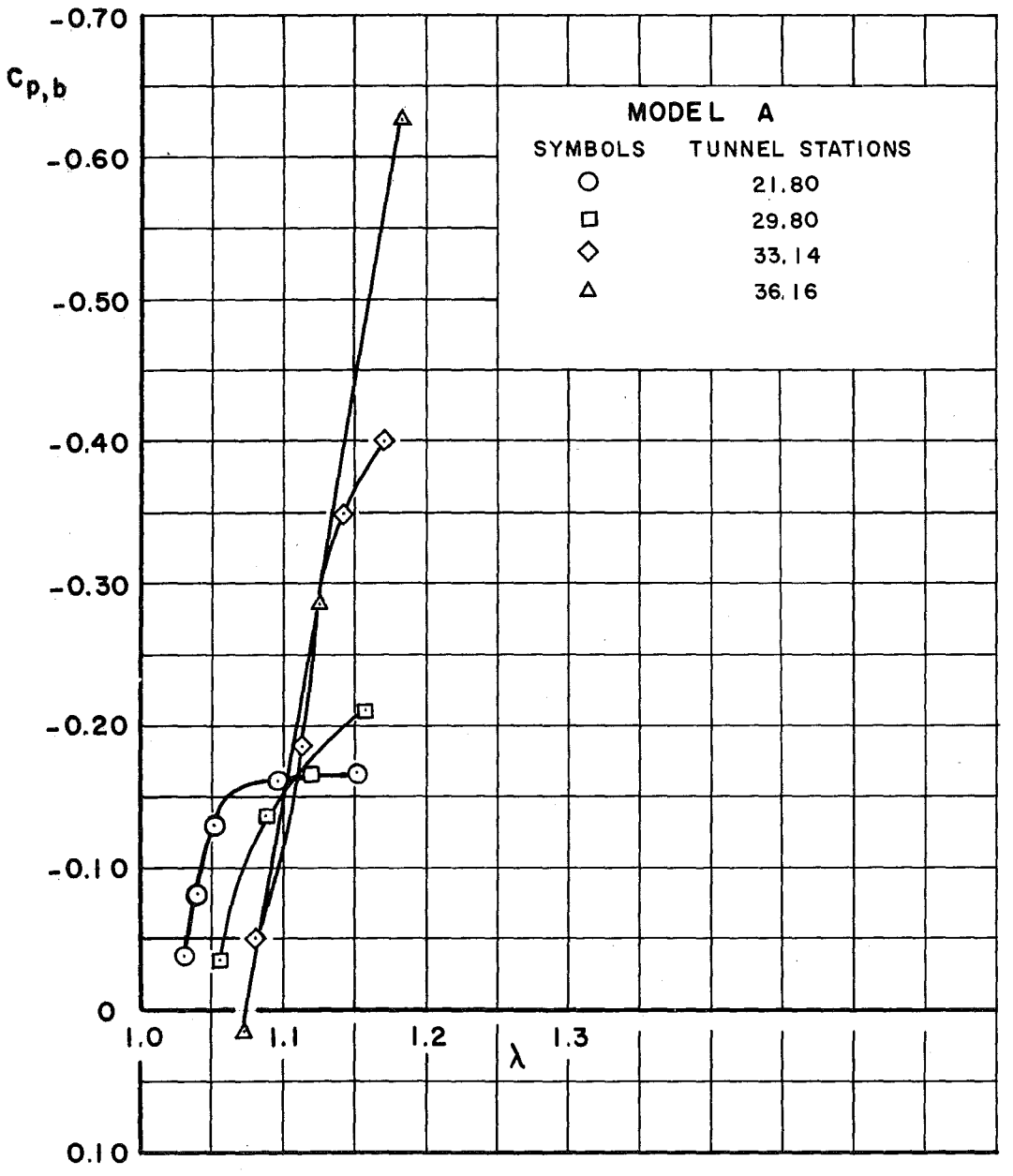


a. Mach Number 0.70

Fig. 8. Base Pressure Coefficient as a Function of Tunnel Pressure Ratio for the Infinite-Length Model A

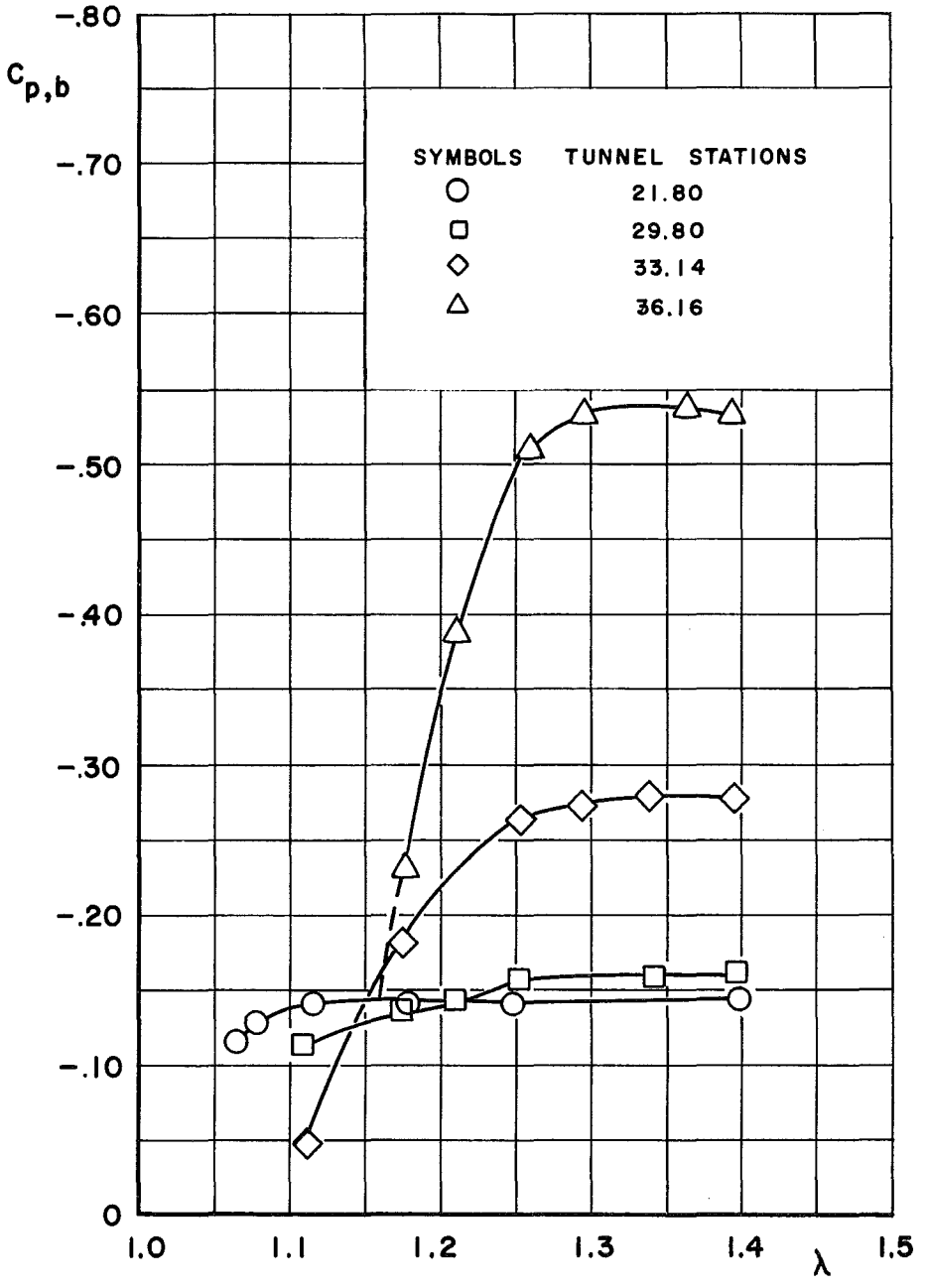


b. Mach Number 0.90

Fig. 8. Continued

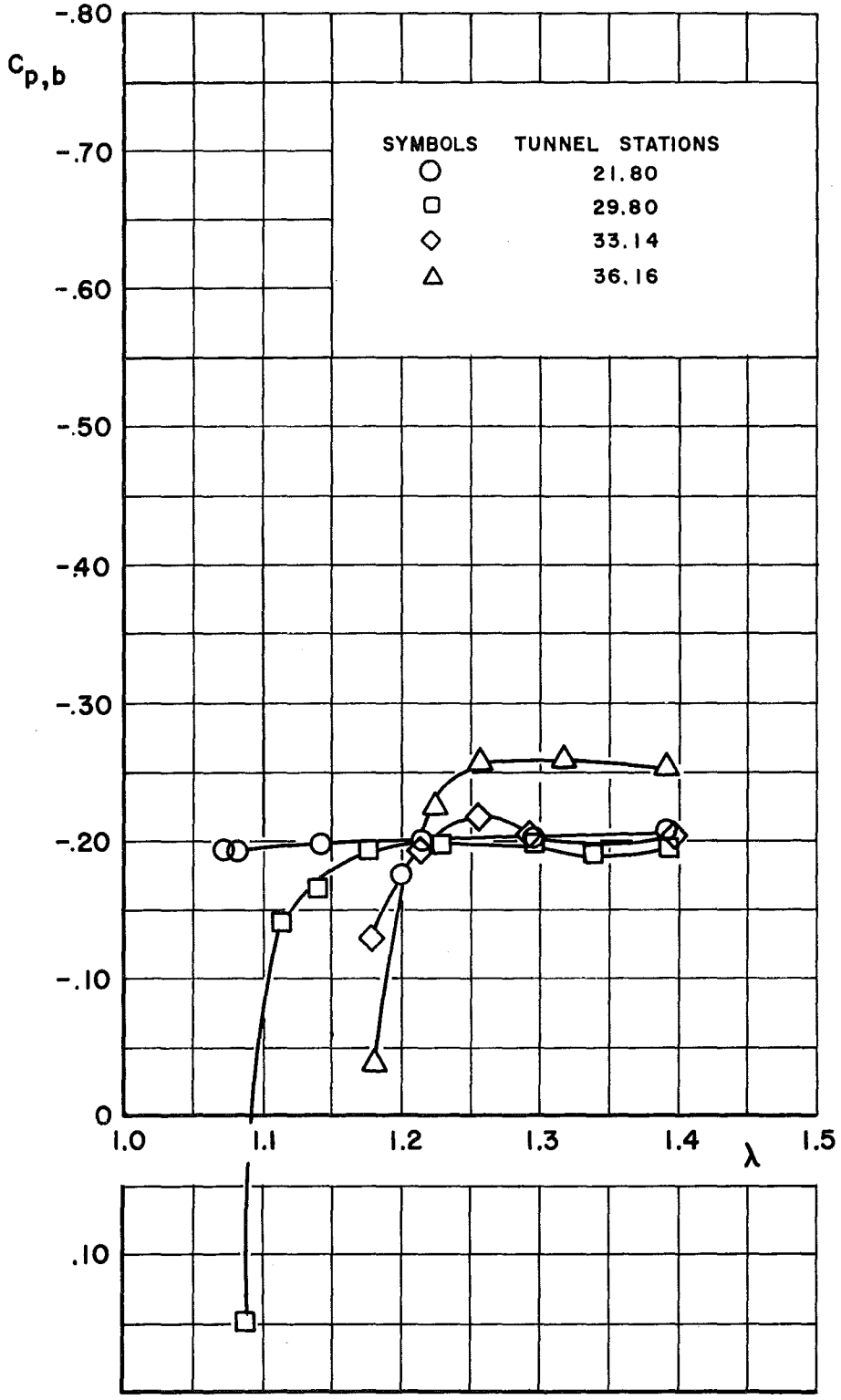


c. Mach Number 1.10

Fig. 8. Continued

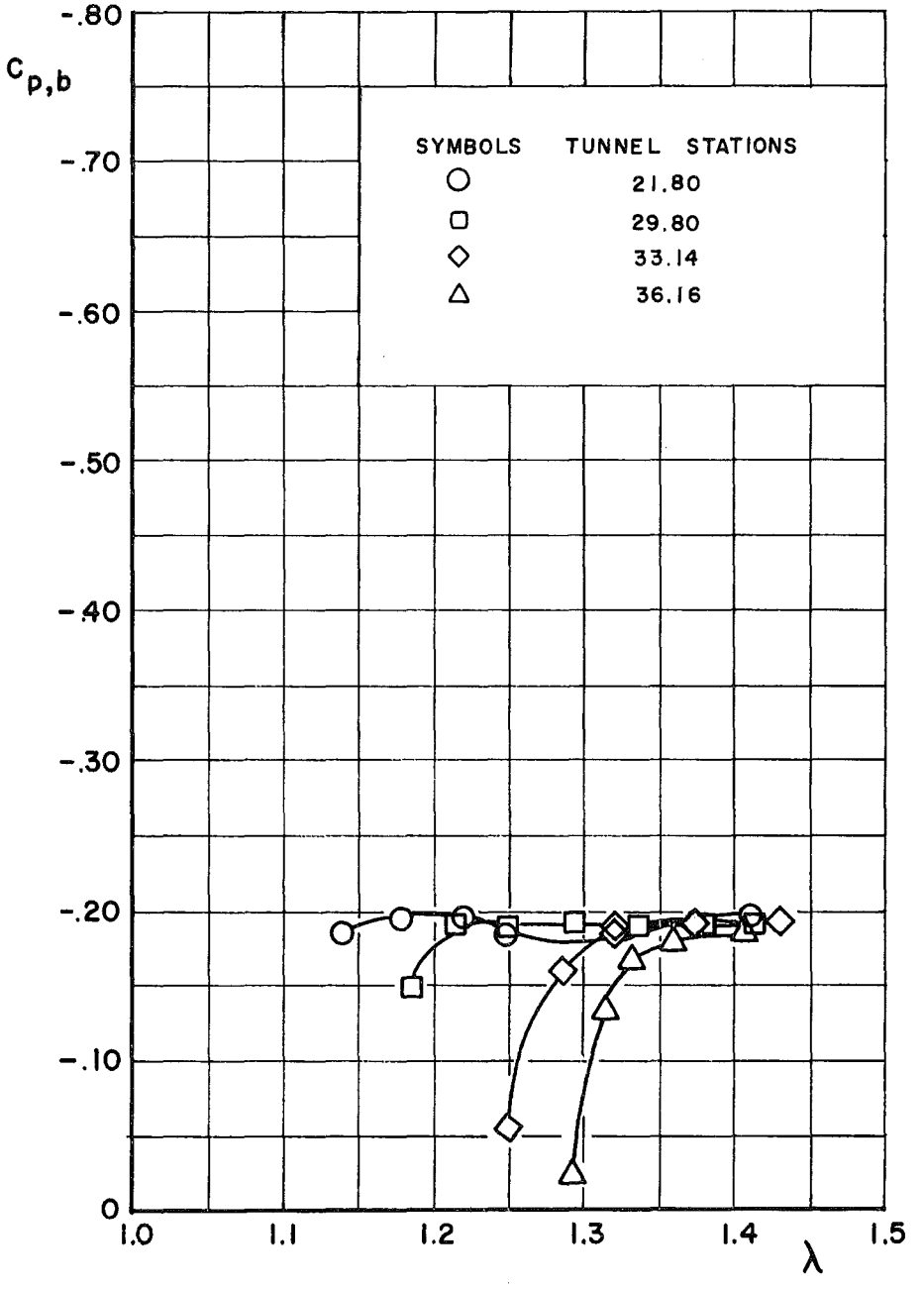


d. Mach Number 1.30

Fig. 8. Concluded

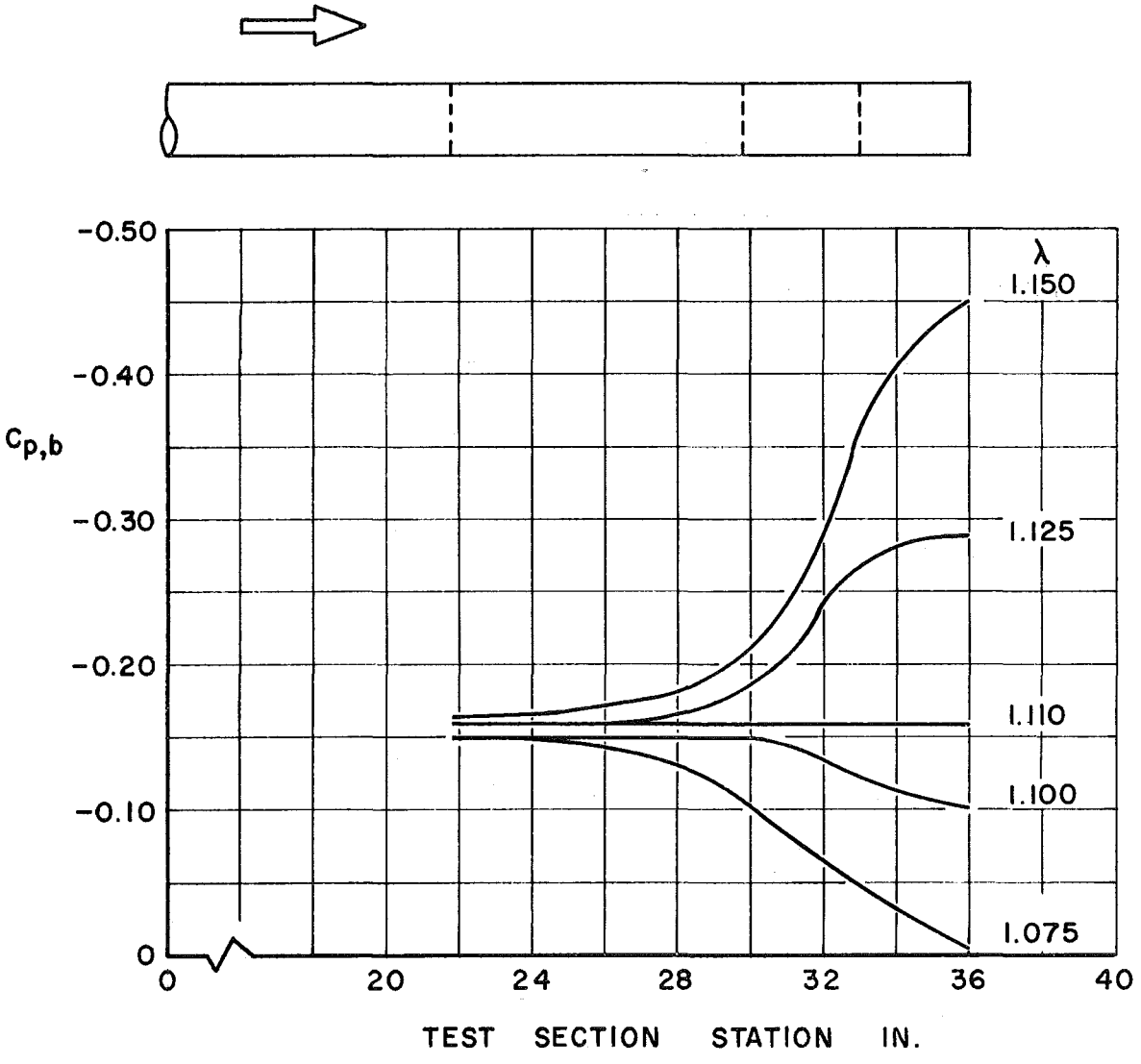


a. Mach Number 0.70

Fig. 9. Base Pressure Coefficient as a Function of Model A Base Location within the Test Section

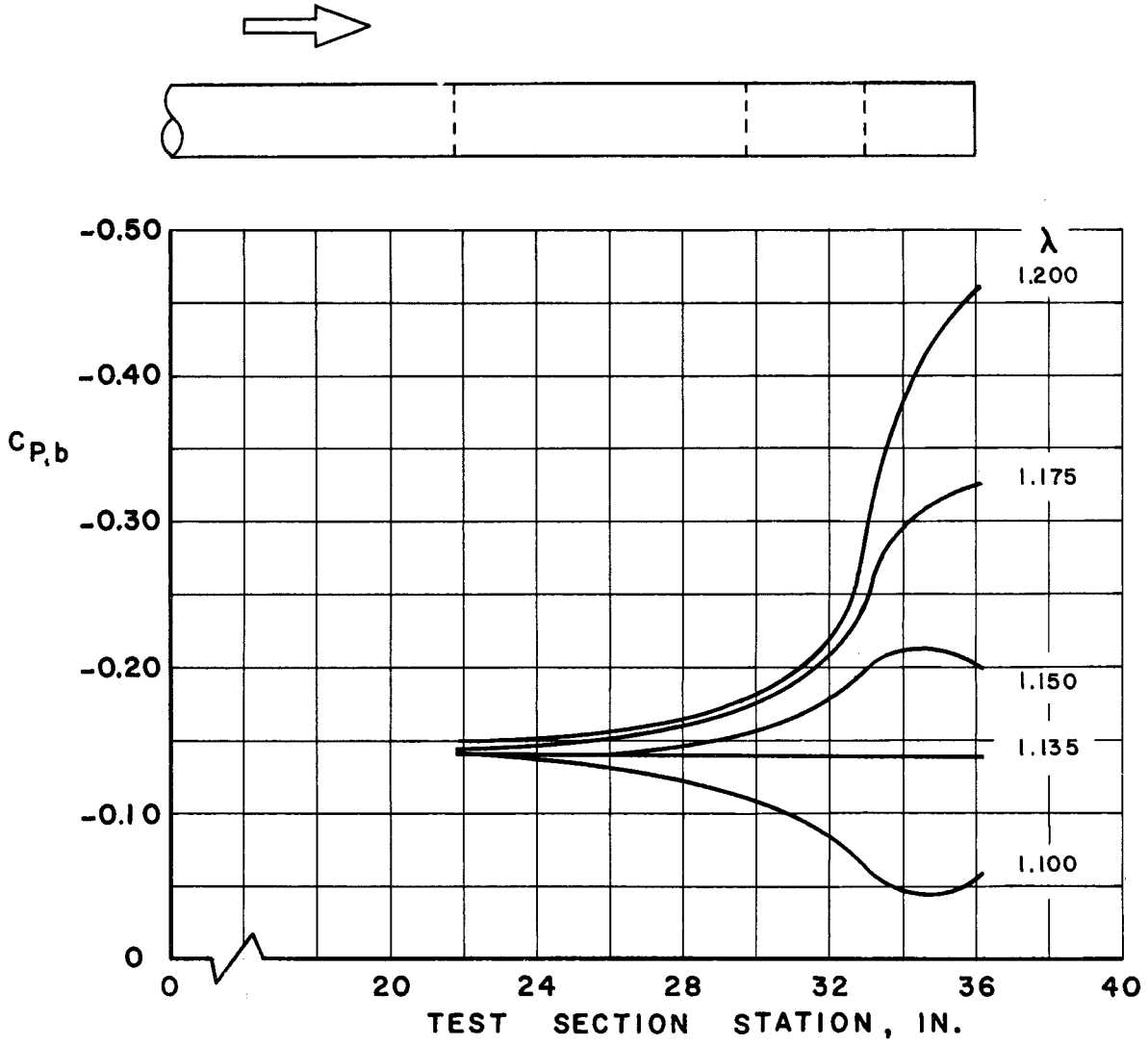


b. Mach Number 0.80

Fig. 9. Continued

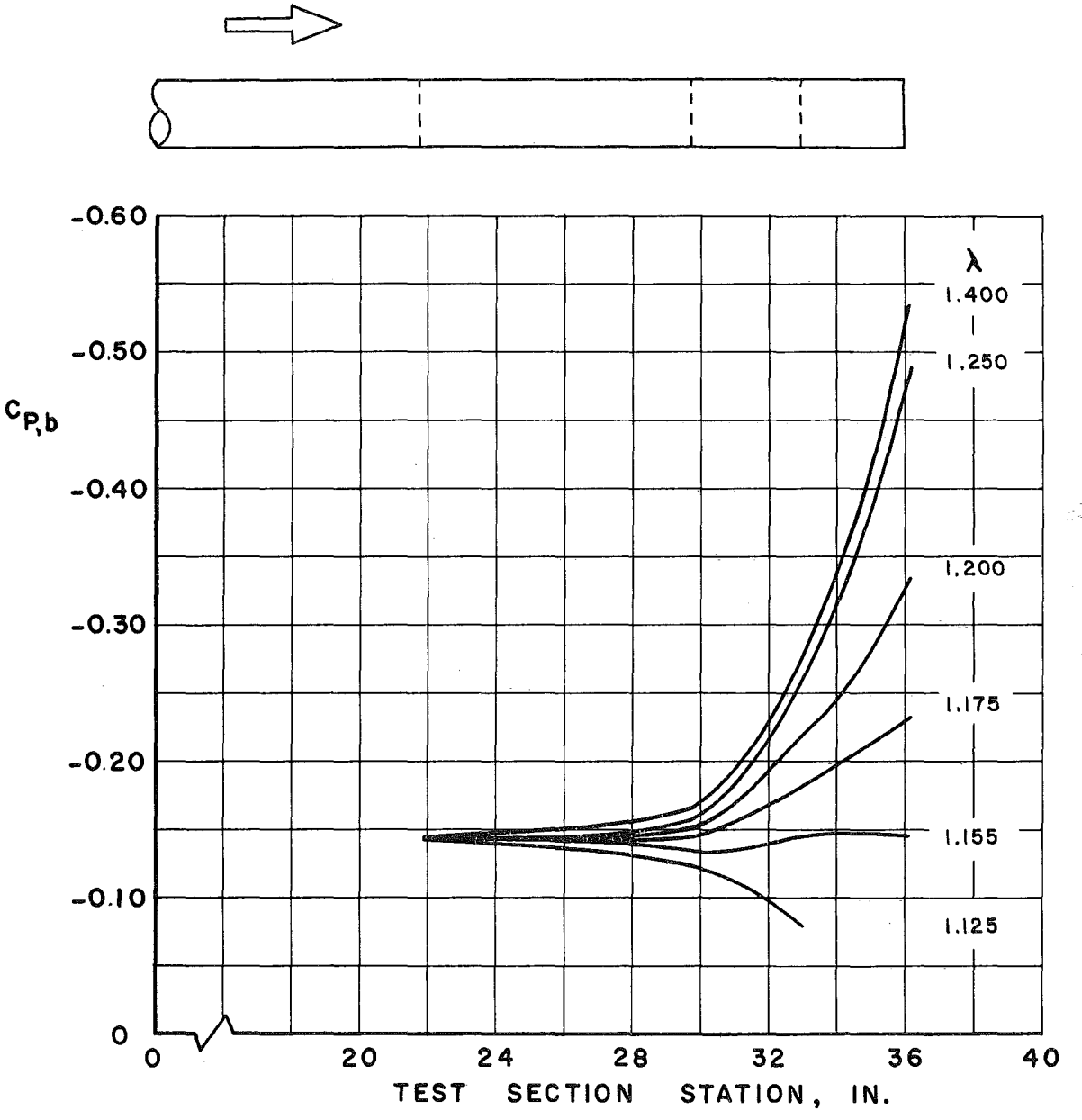


c. Mach Number 0.90

Fig. 9. Continued

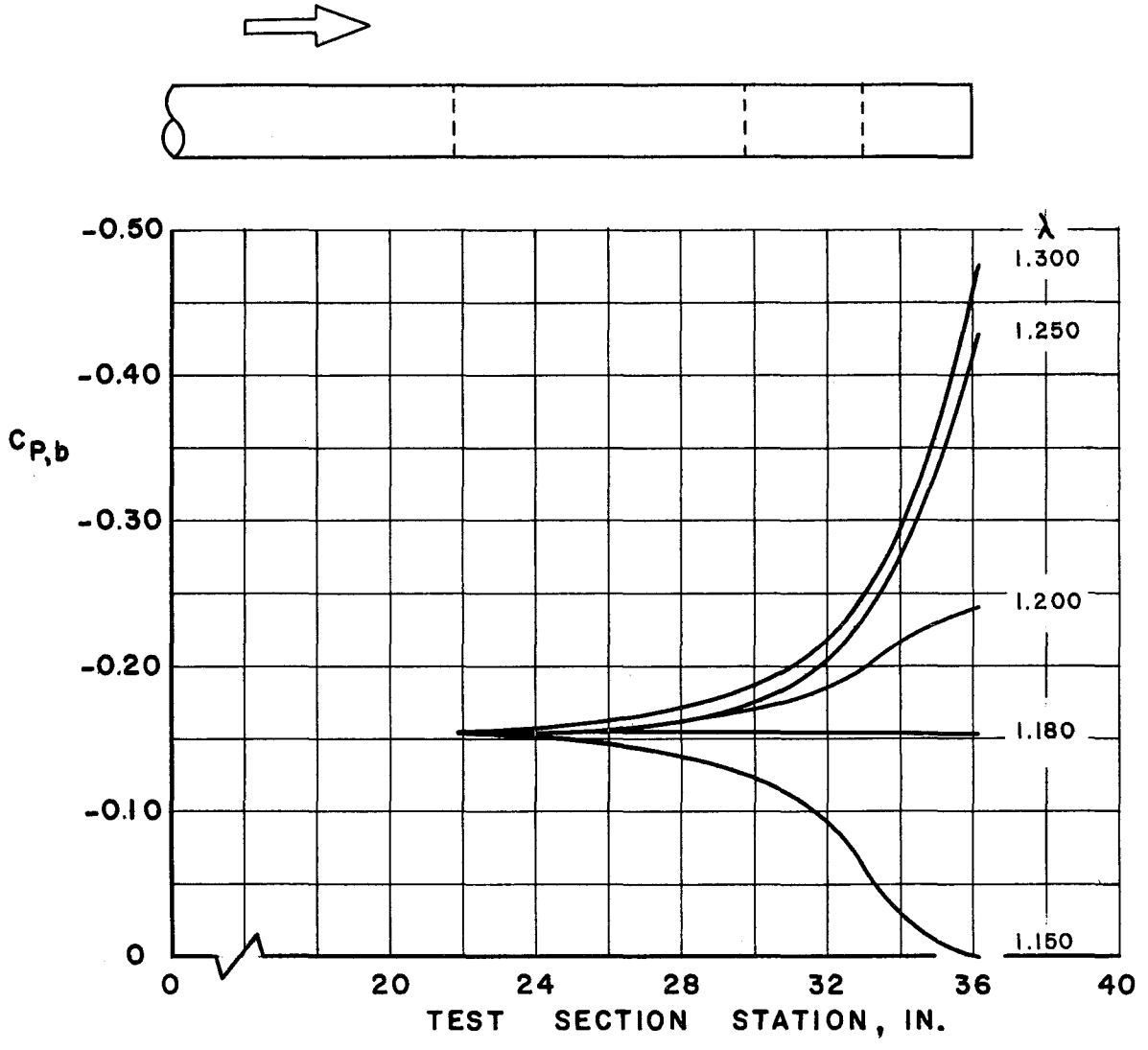


d. Mach Number 0.95

Fig. 9. Continued

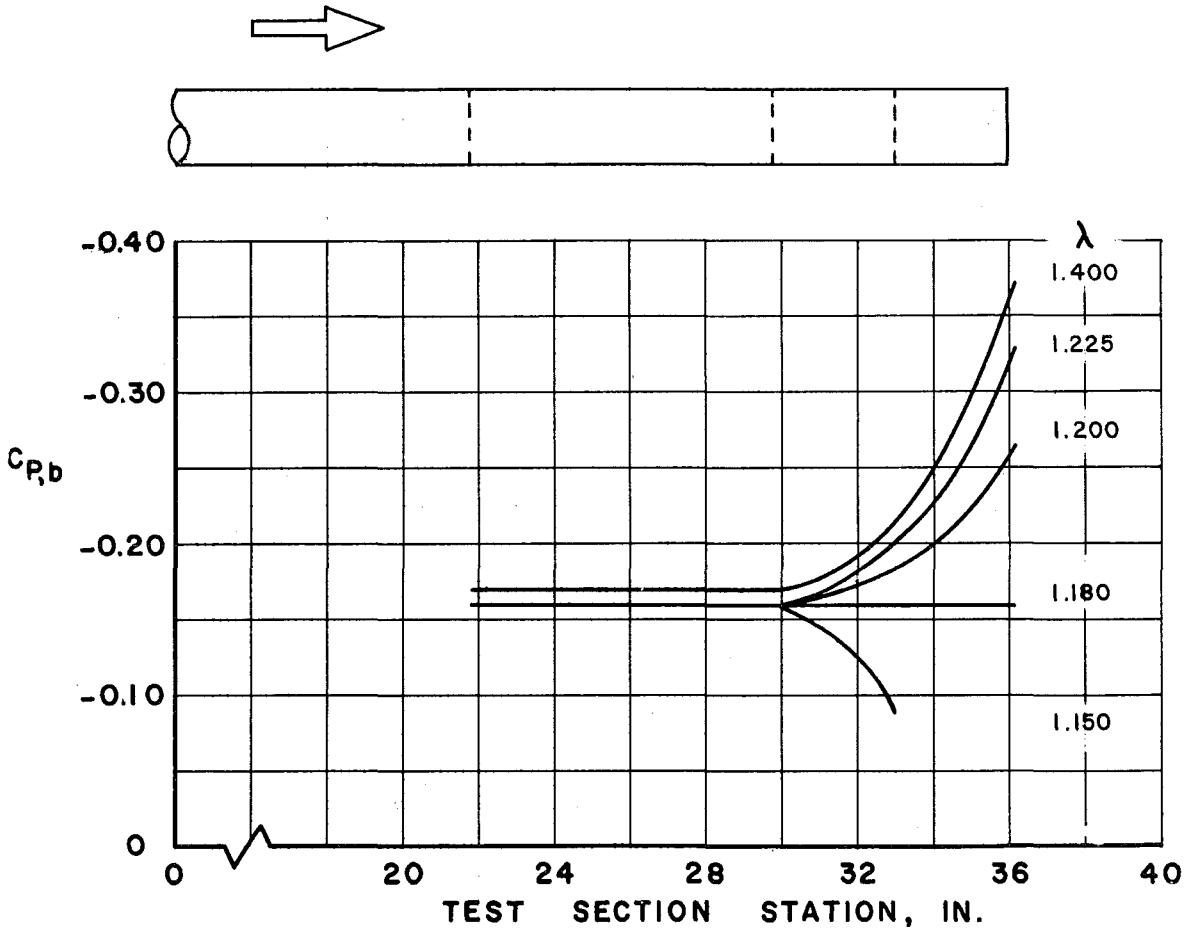


e. Mach Number 1.00

Fig. 9. Continued

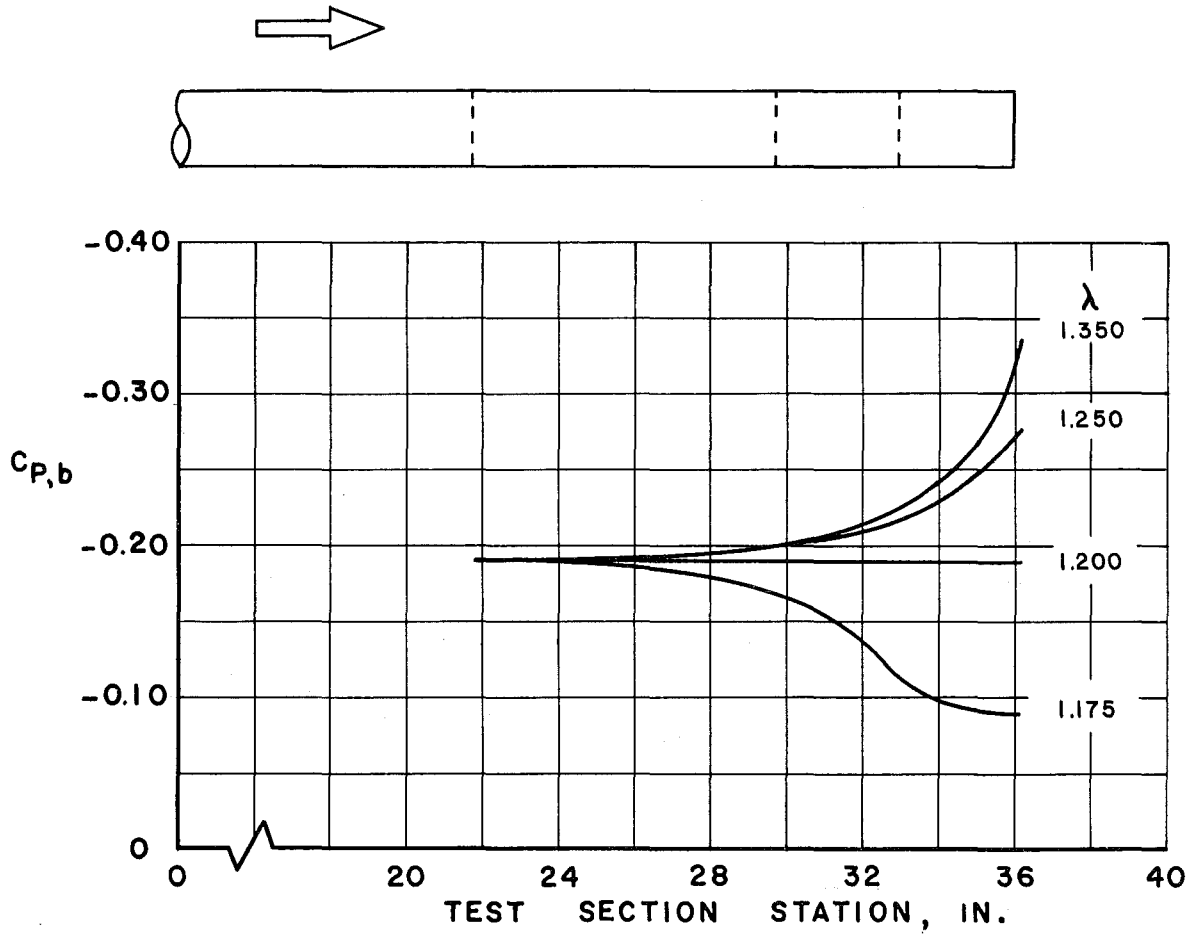


f. Mach Number 1.05

Fig. 9. Continued

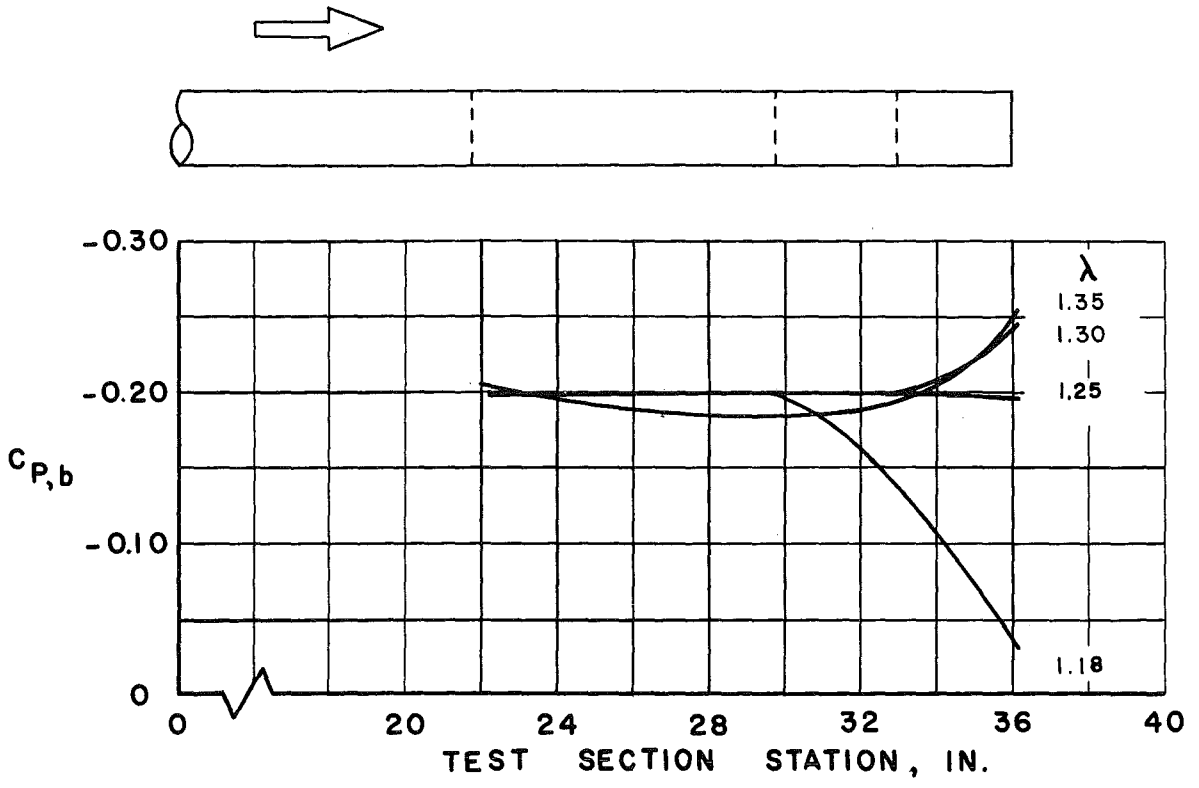


g. Mach Number 1.10

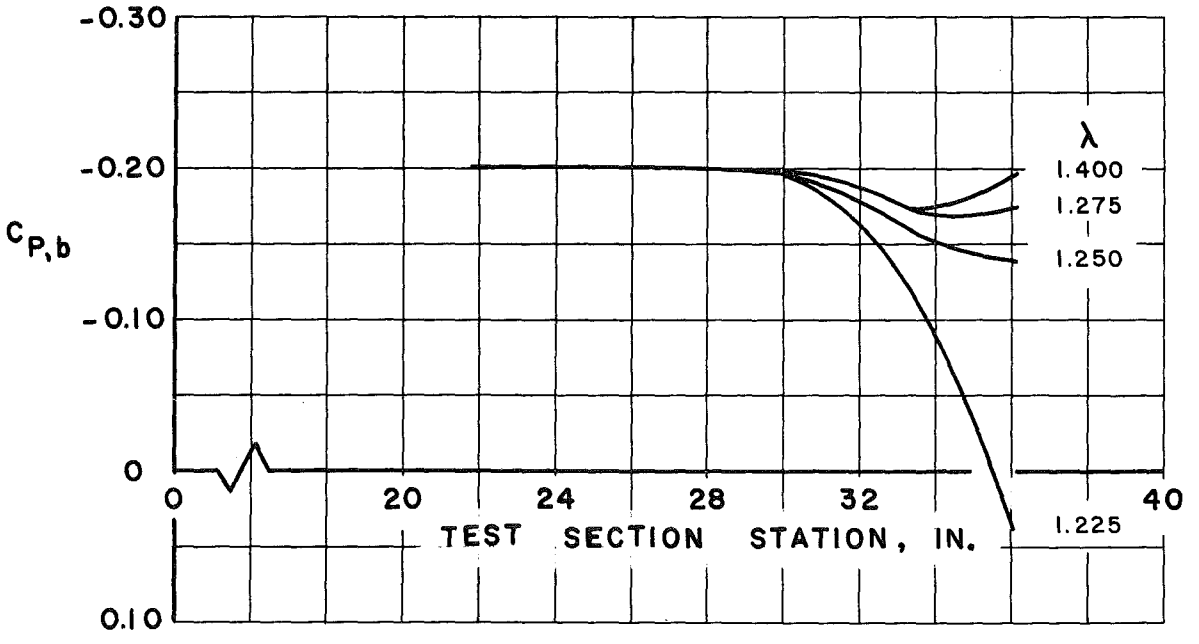


h. Mach Number 1.20

Fig. 9. Continued

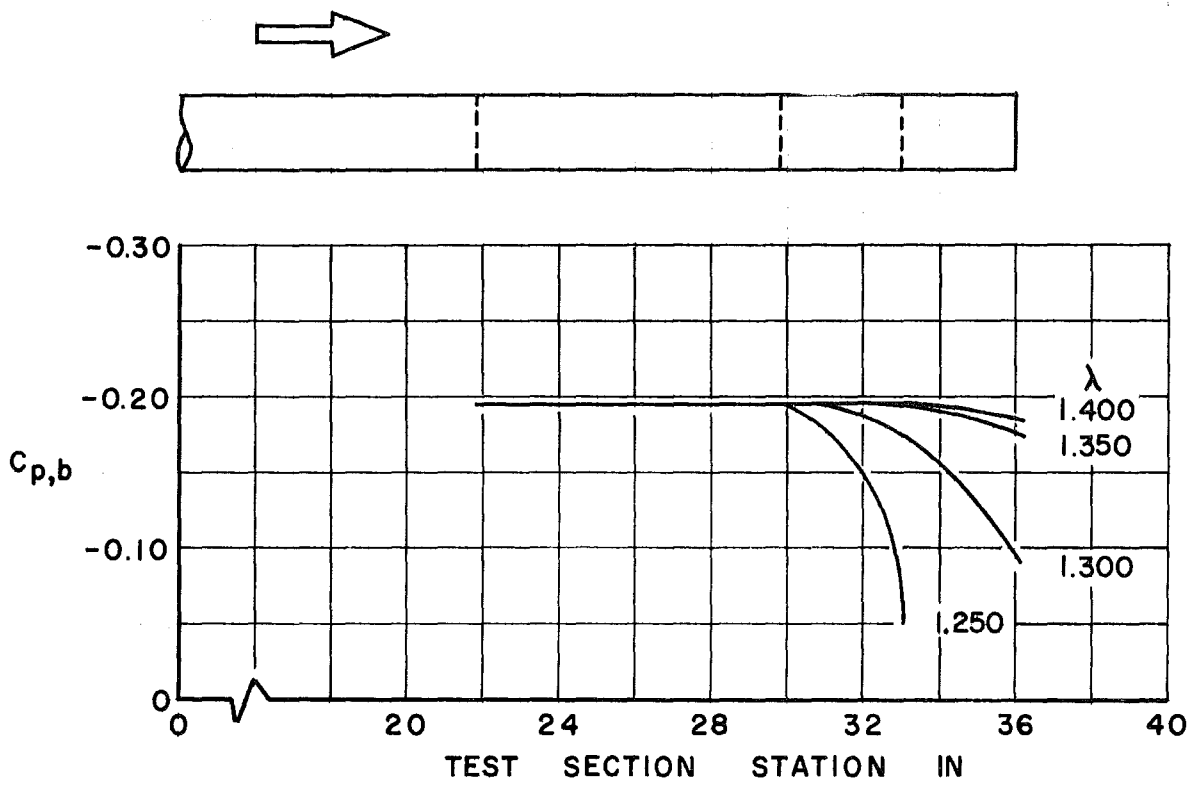


i. Mach Number 1.30

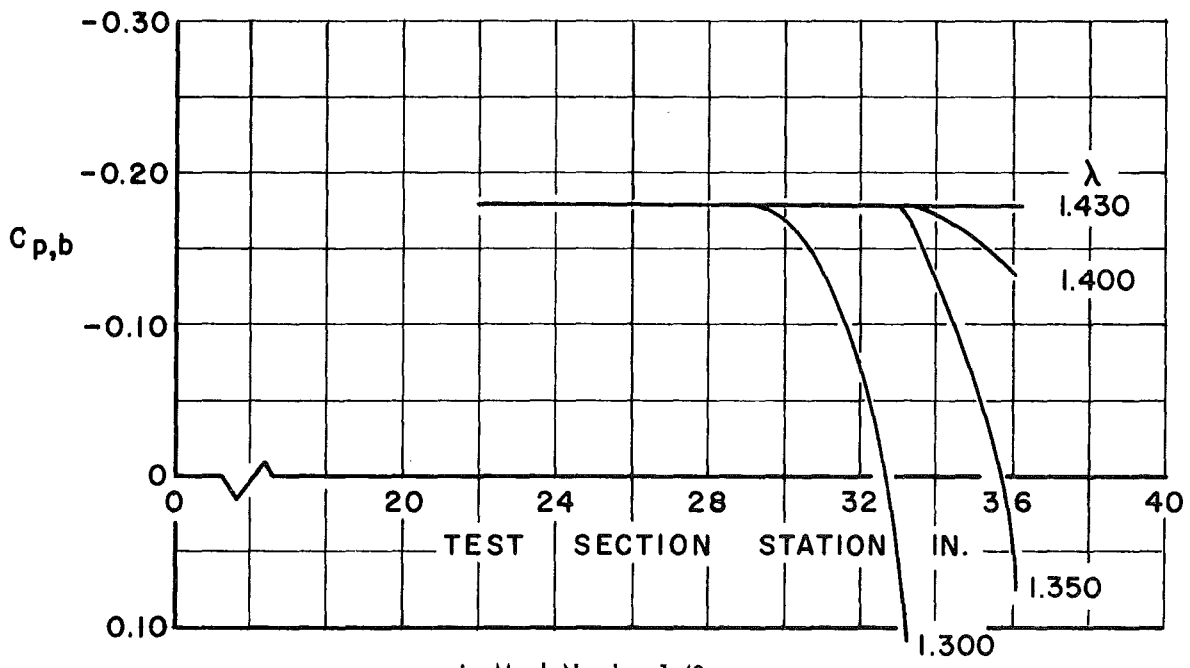


j. Mach Number 1.40

Fig. 9. Concluded

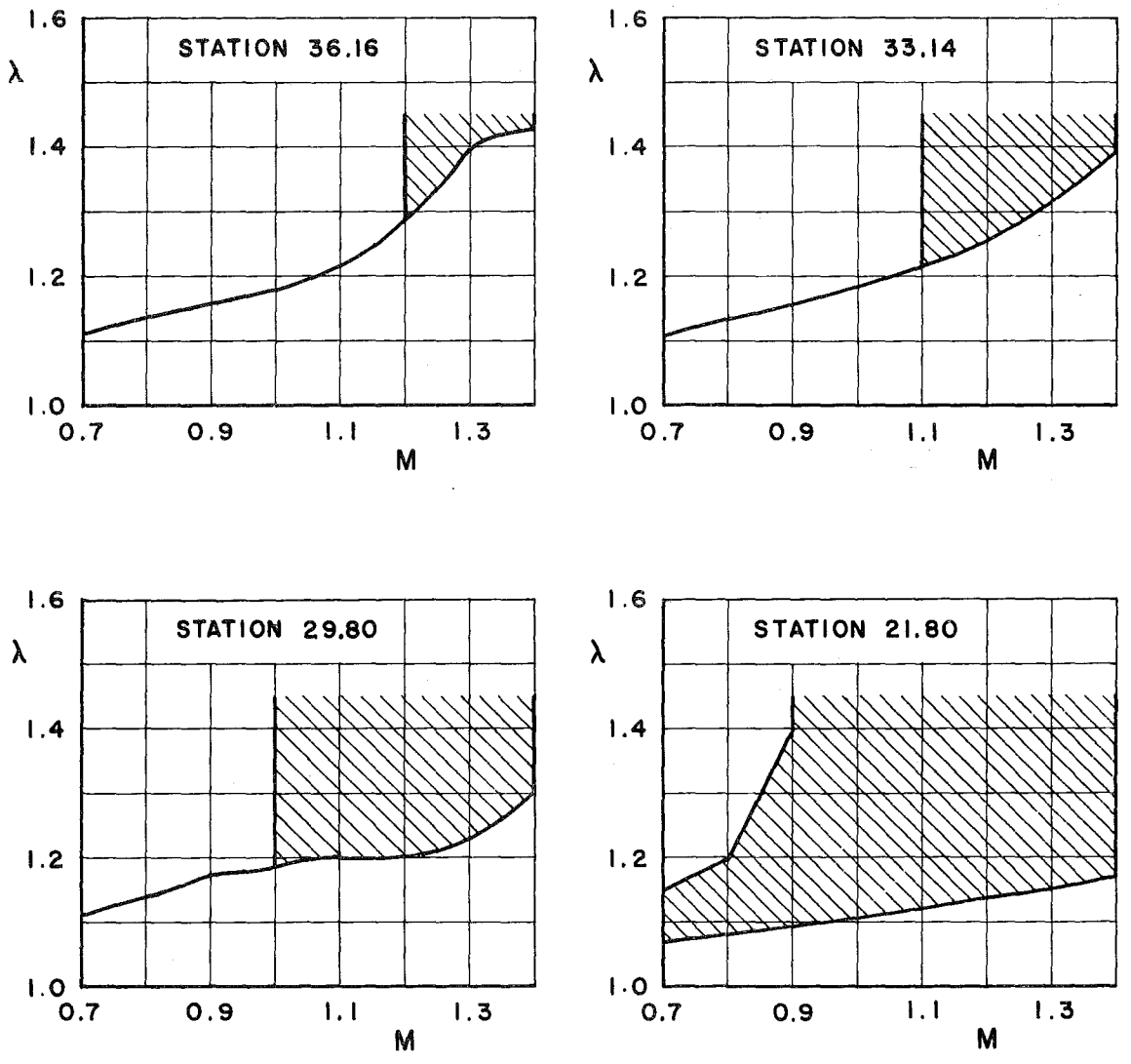


Fig. 10. Correct Operating Tunnel Pressure Ratio as a Function of Mach Number for the Infinite-Length Model A

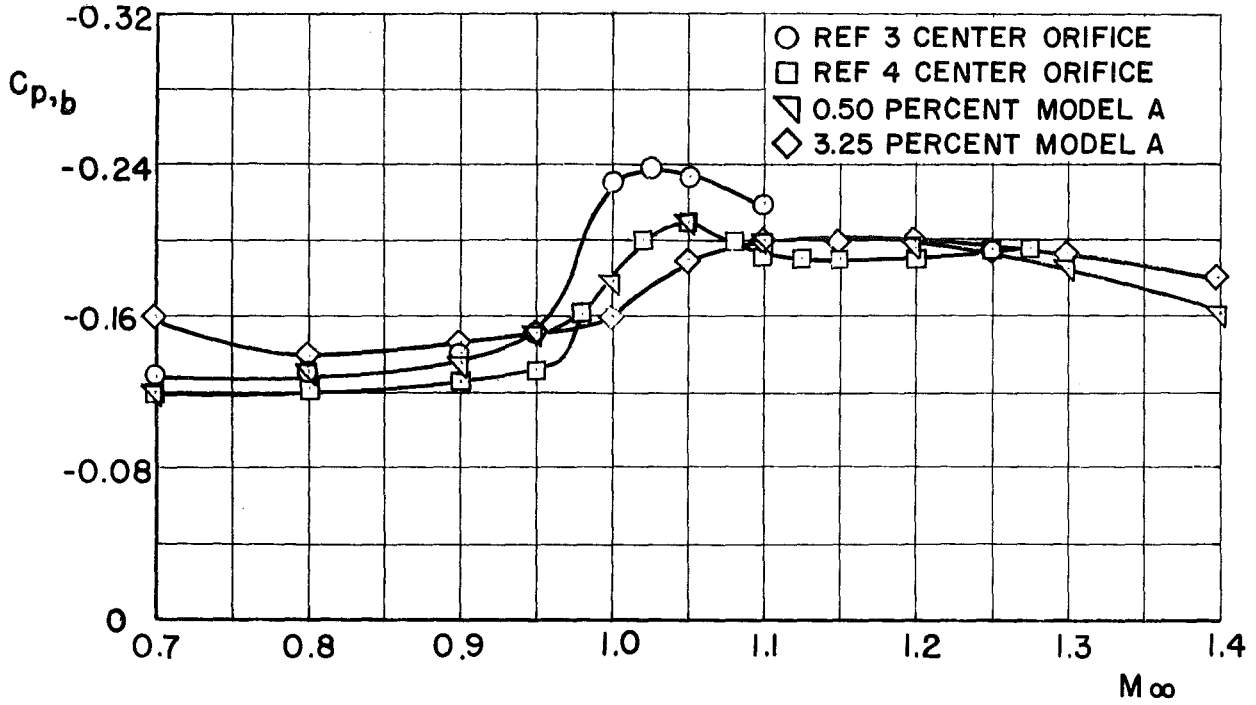


Fig. 11. Base Pressure Coefficient as a Function of Mach Number for the Infinite-Length Model A and Free-Flight Data

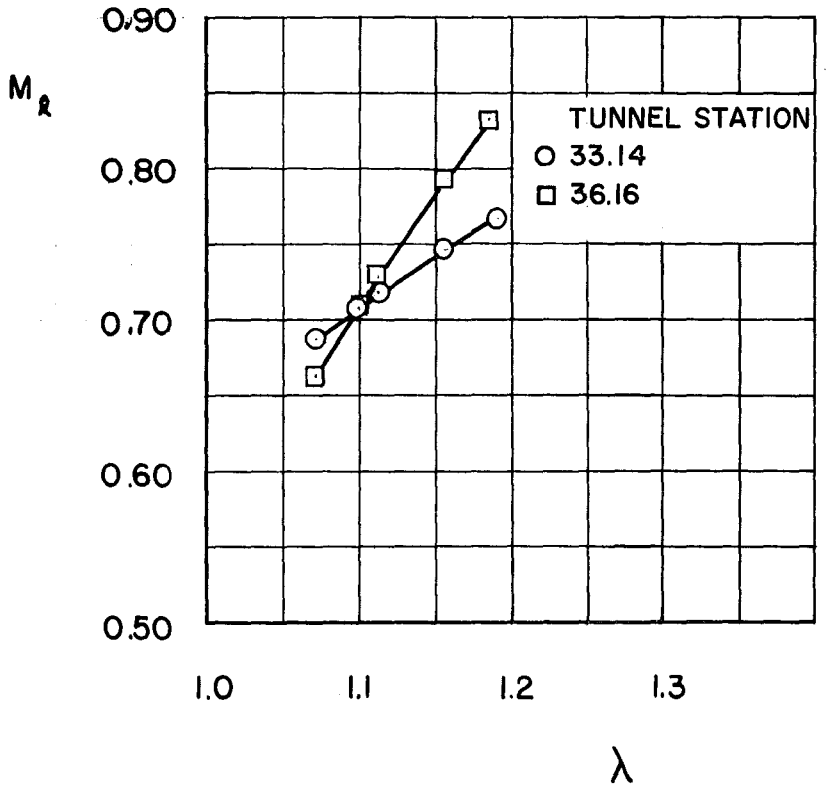


Fig. 12. Variation of the Local Mach Number as a Function of Tunnel Pressure Ratio for the Infinite-Length Model A at Free-Stream Mach Number 0.70

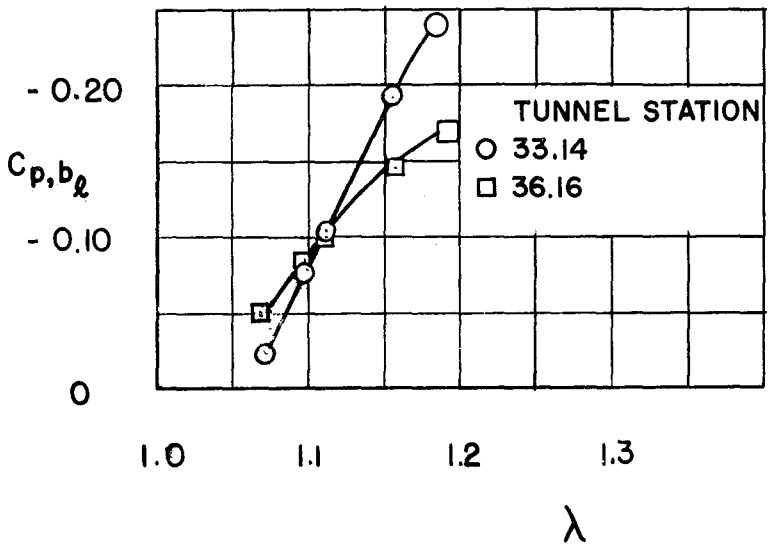


Fig. 13. Variation of the Local Base-Pressure Coefficient as a Function of Tunnel Pressure Ratio for the Infinite-Length Model A at Free-Stream Mach Number 0.70

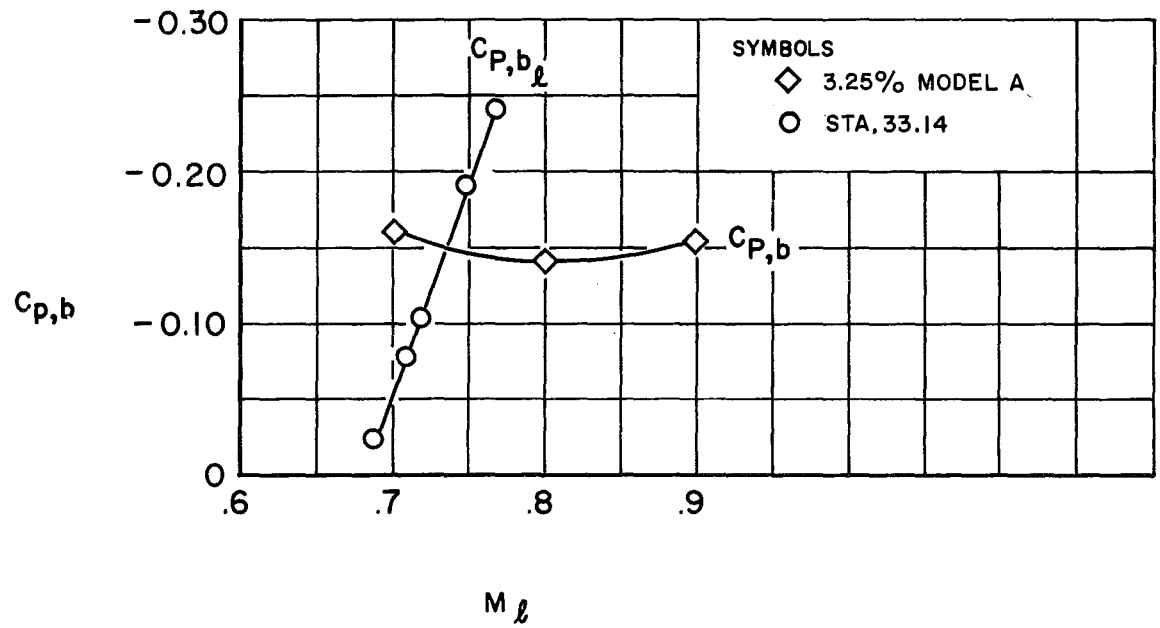


Fig. 14. Comparison of Base Pressure Coefficients Based on Local and Free-Stream Conditions for Model A at Station 33.14 and Free-Stream Mach Number 0.70

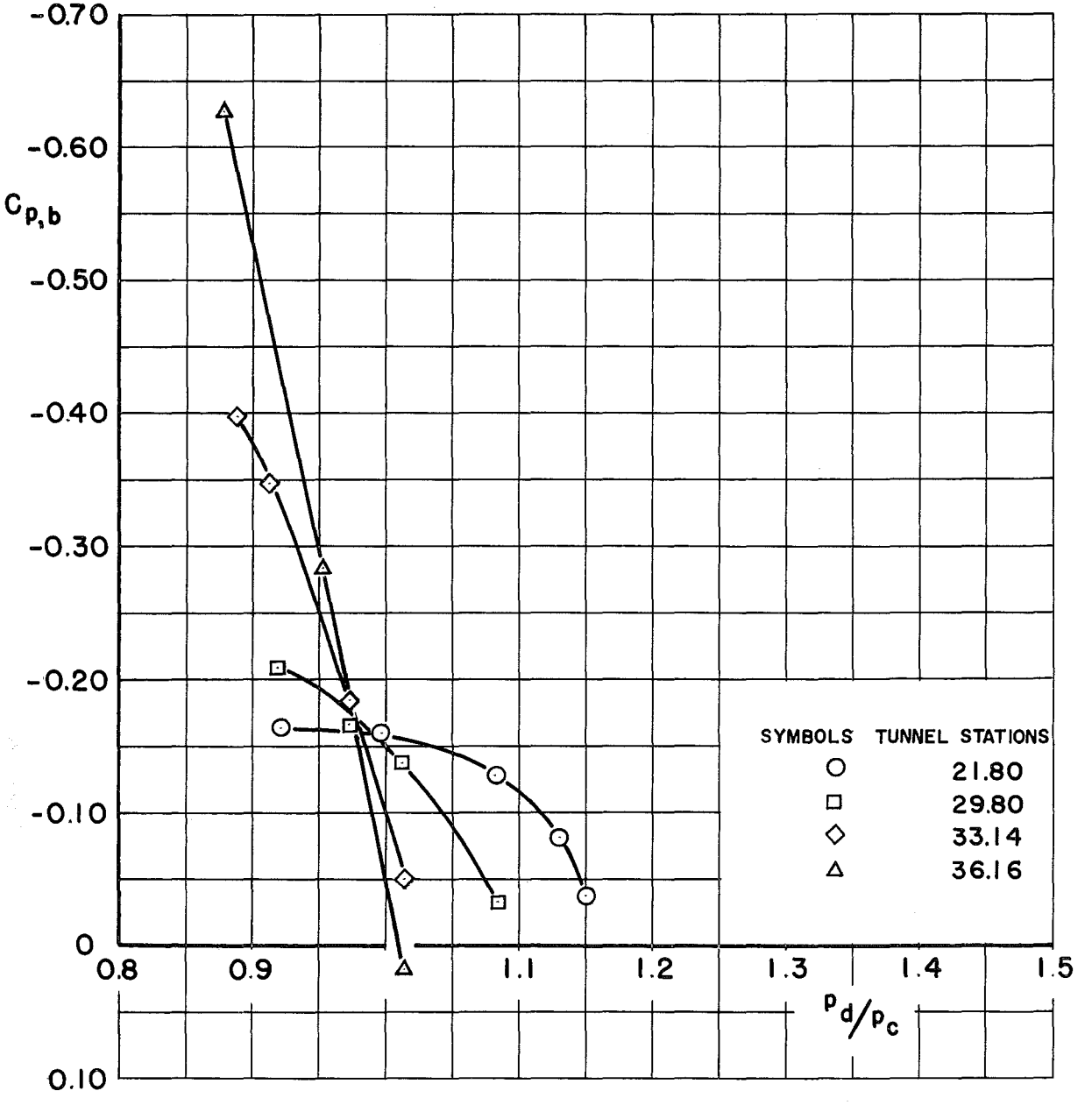


a. Mach Number 0.70

Fig. 15. Base Pressure Coefficient as a Function of $p_d/p_c$ for the Infinite-Length Model A

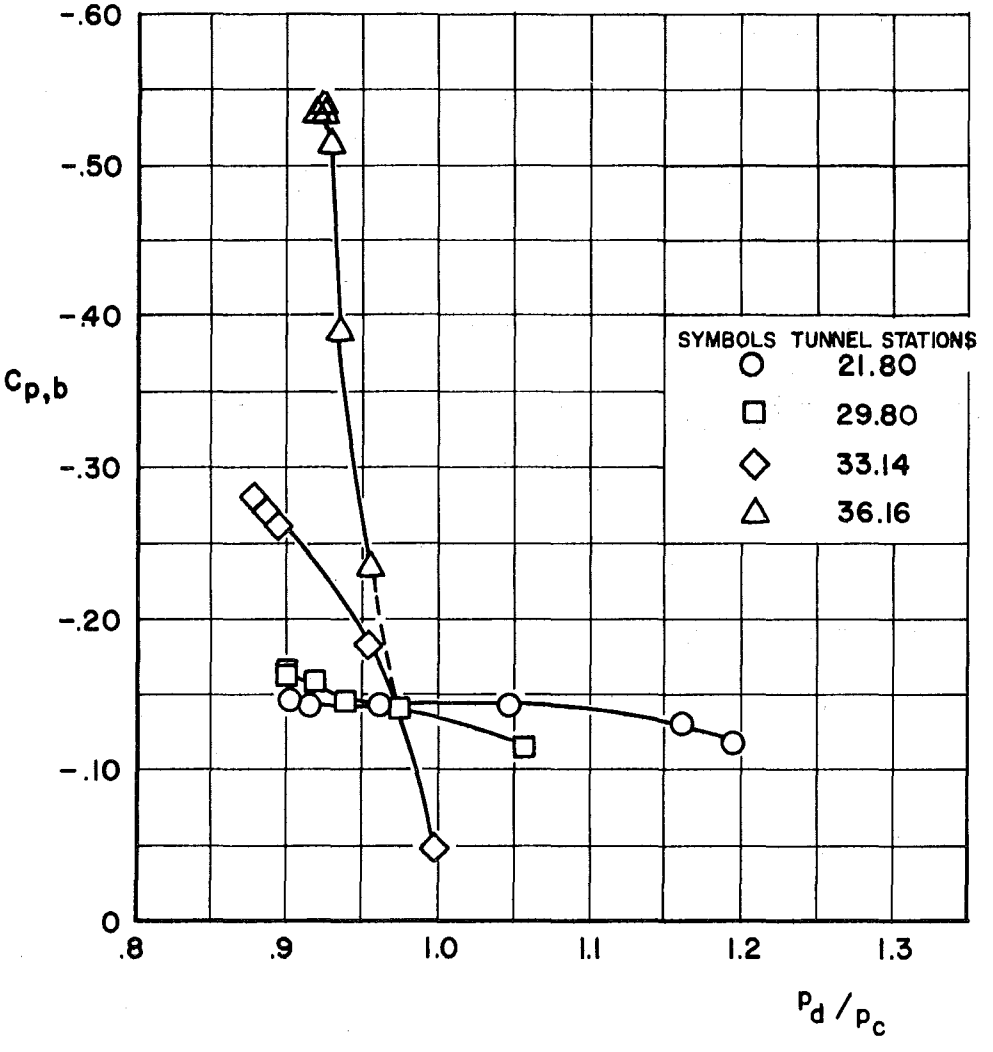


b. Mach Number 0.90

Fig. 15. Continued

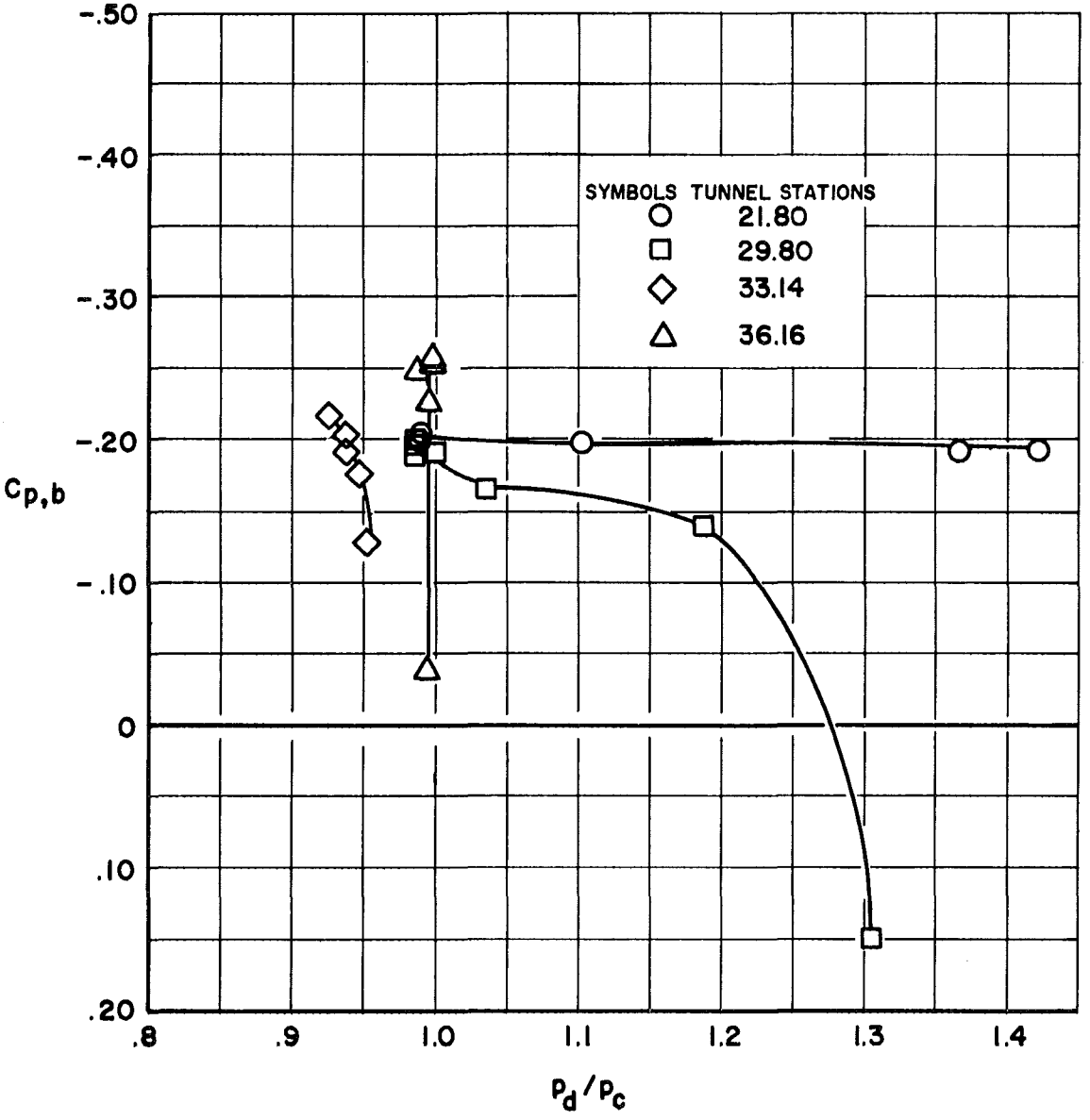


c. Mach Number 1.10

Fig. 15. Continued

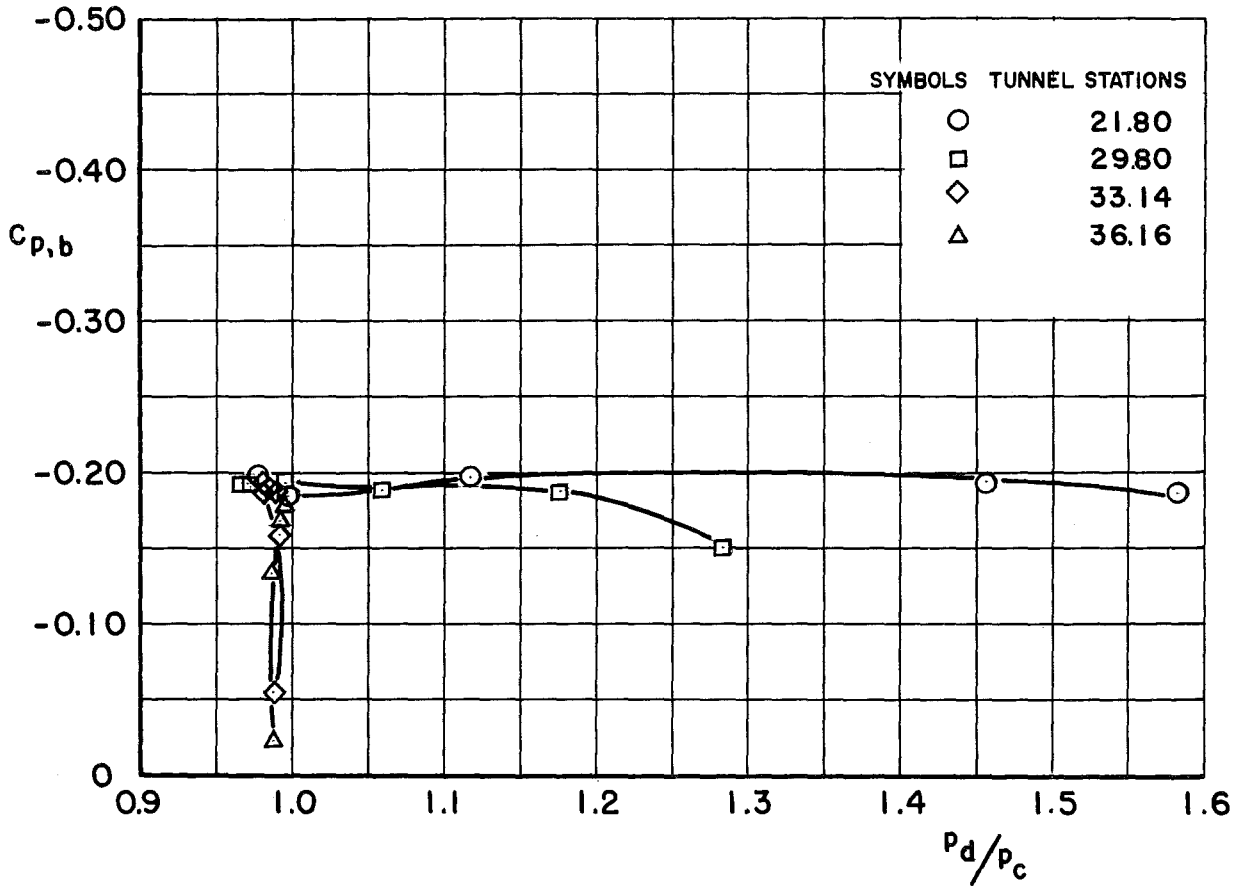


d. Mach Number 1.30

Fig. 15. Concluded

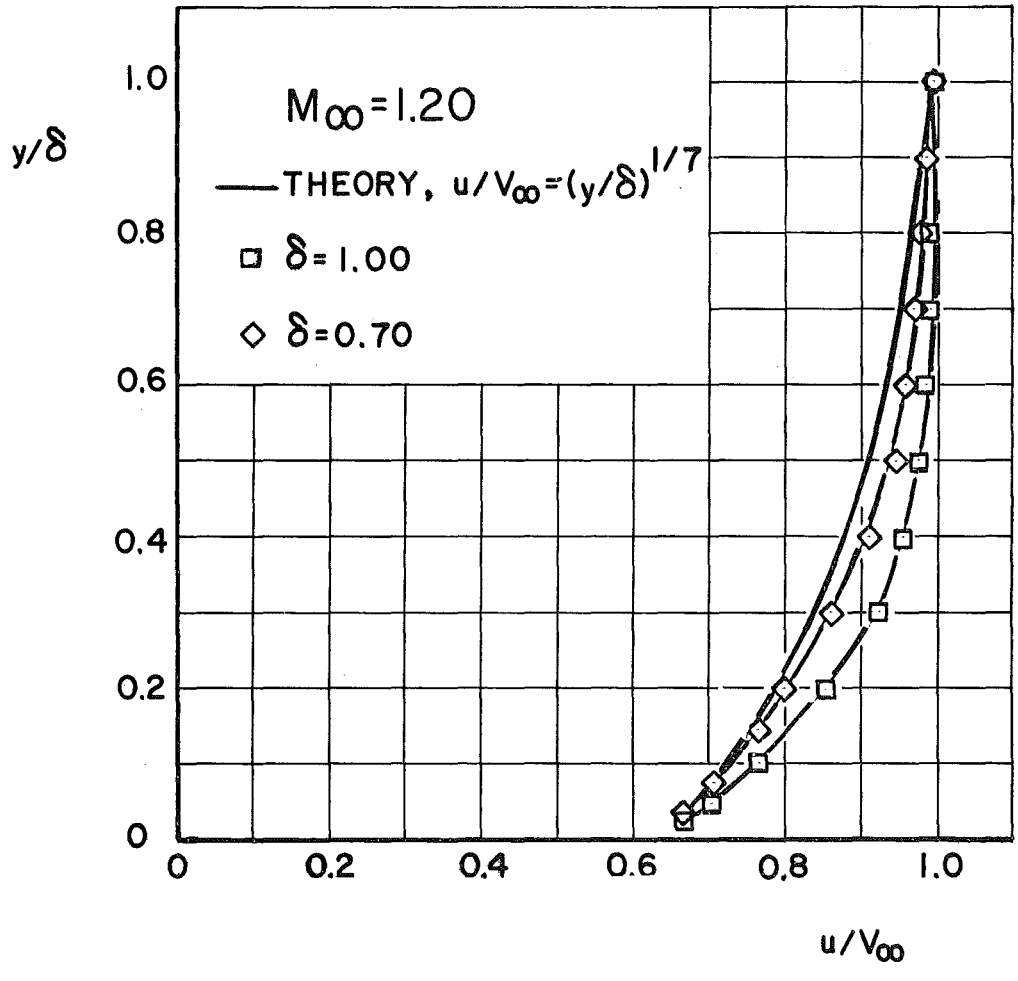


Fig. 16. Boundary Layer Profile Determined at Tunnel Station 15.30 on the Model Support Tube at a Mach Number of 1.20

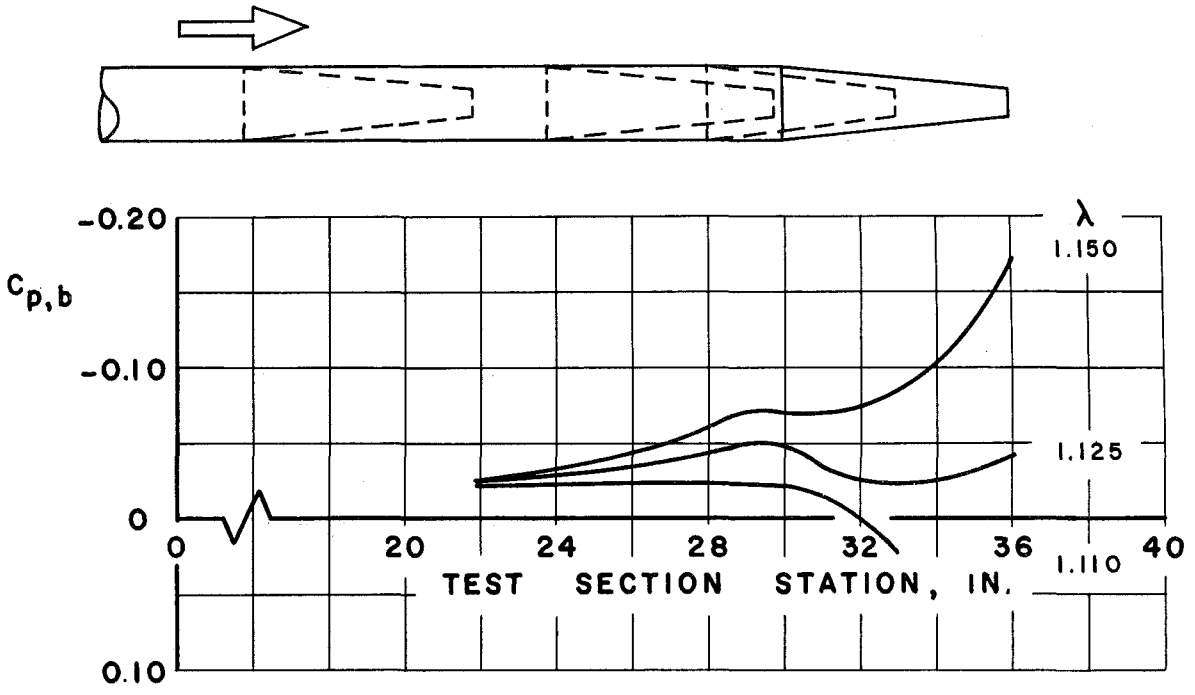


a. Mach Number 0.70

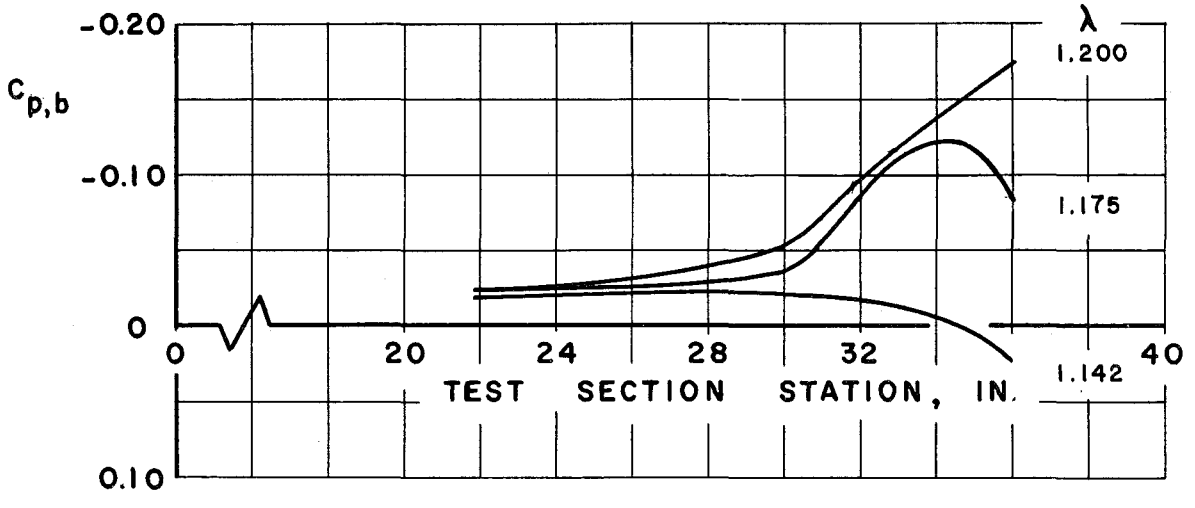


b. Mach Number 0.80

Fig. 17. Base Pressure Coefficient as a Function of Model B Base Location within the Test Section

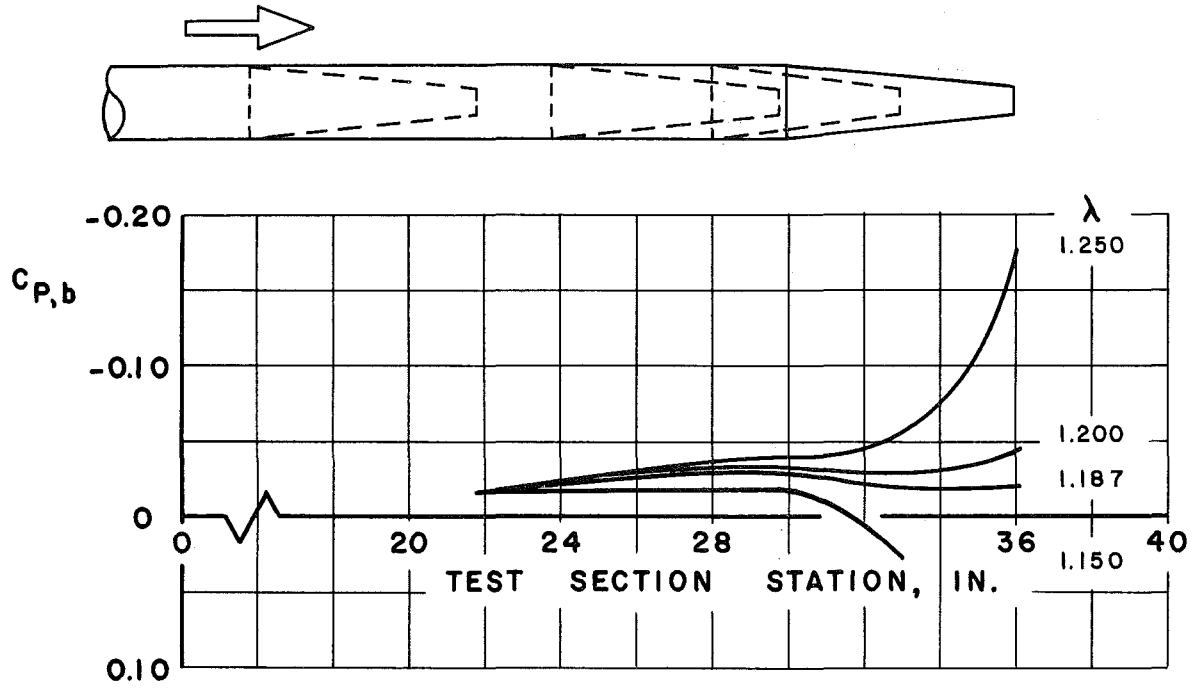


c. Mach Number 0.90

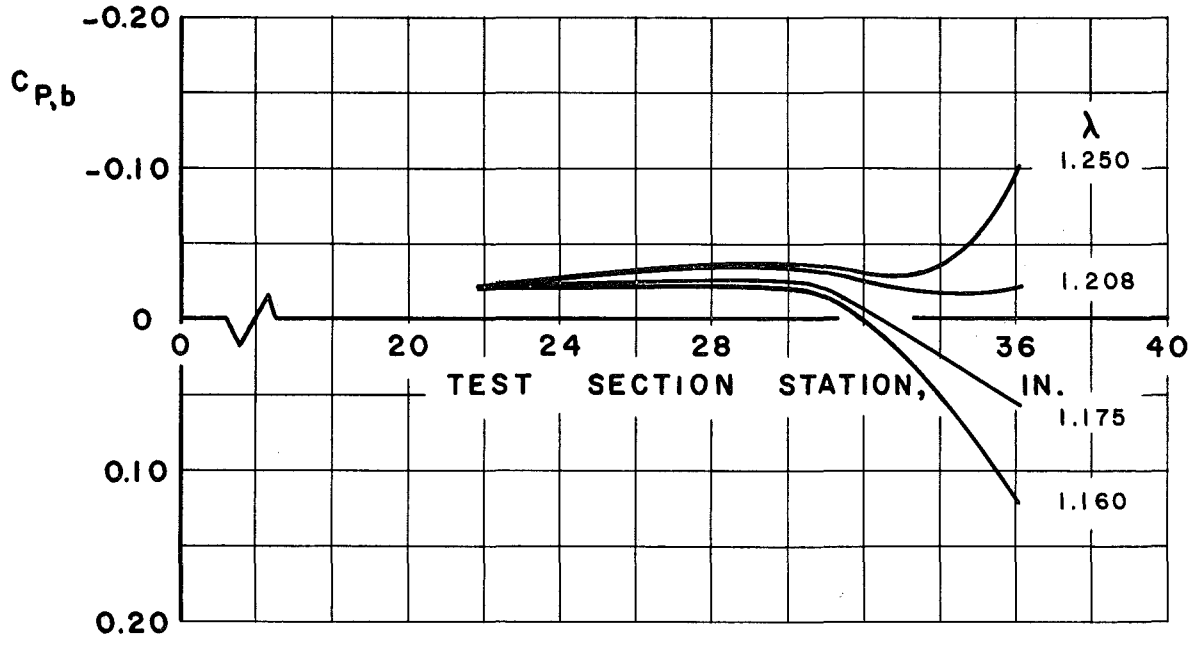


d. Mach Number 0.95

Fig. 17. Continued

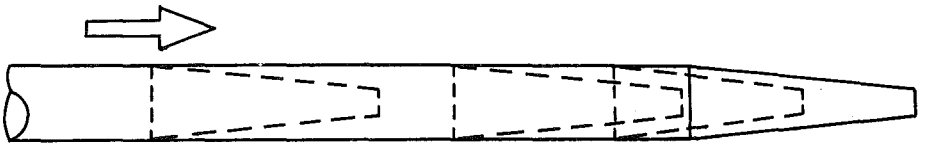

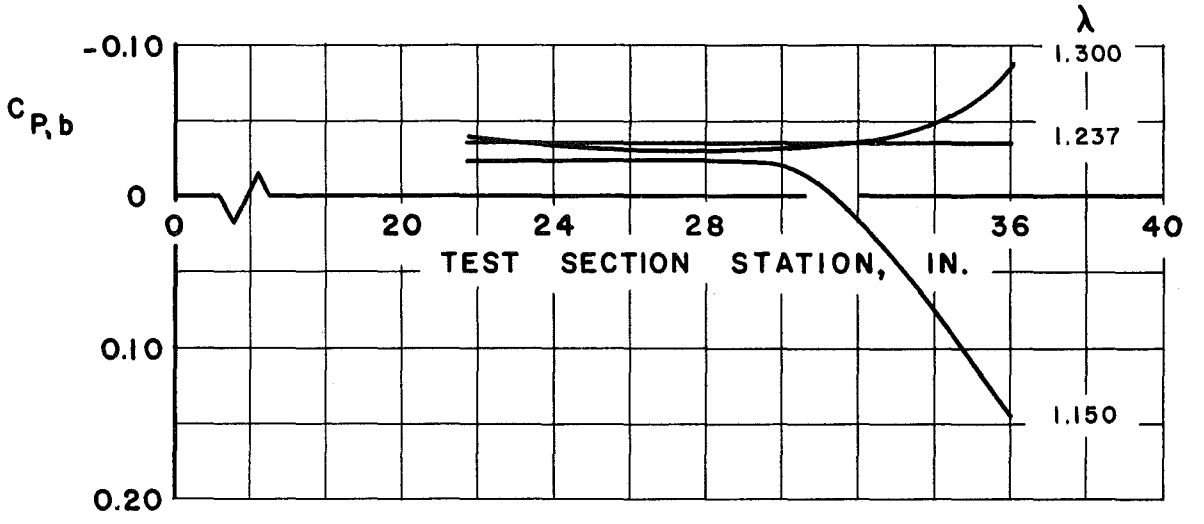


e. Mach Number 1.00

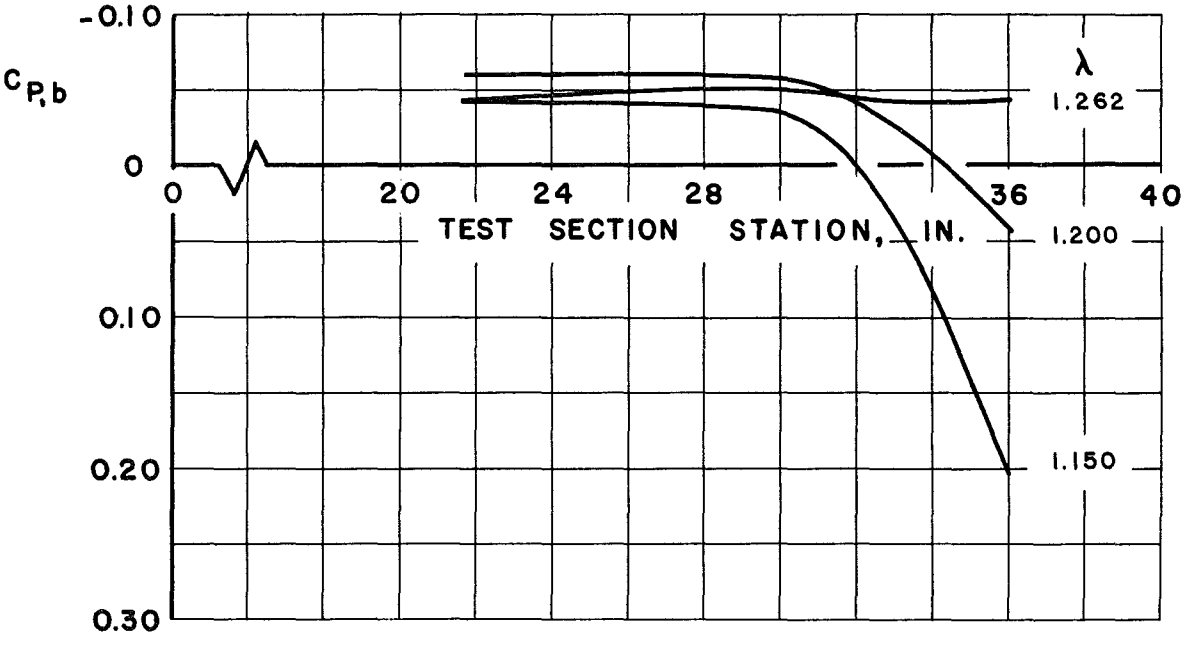


f. Mach Number 1.05

Fig. 17. Continued

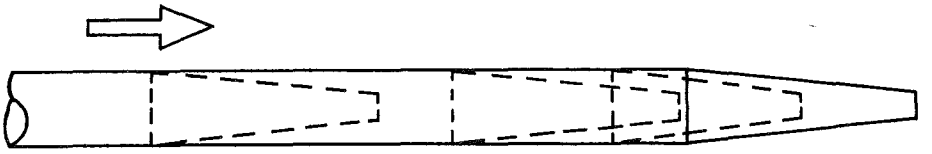

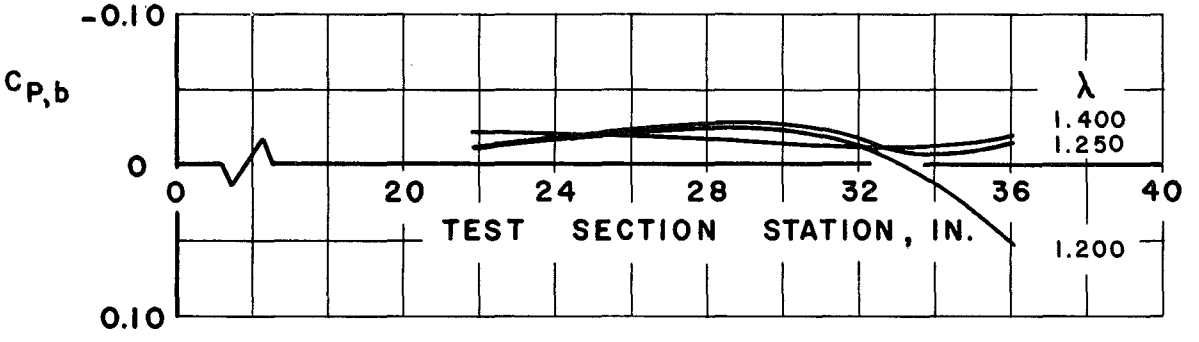


g. Mach Number 1.10

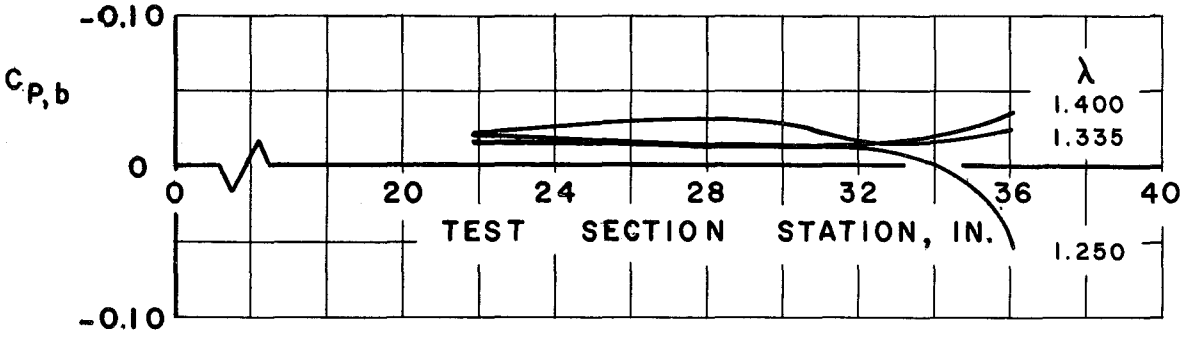


h. Mach Number 1.20

Fig. 17. Continued

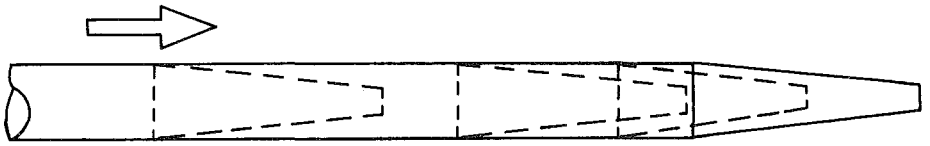

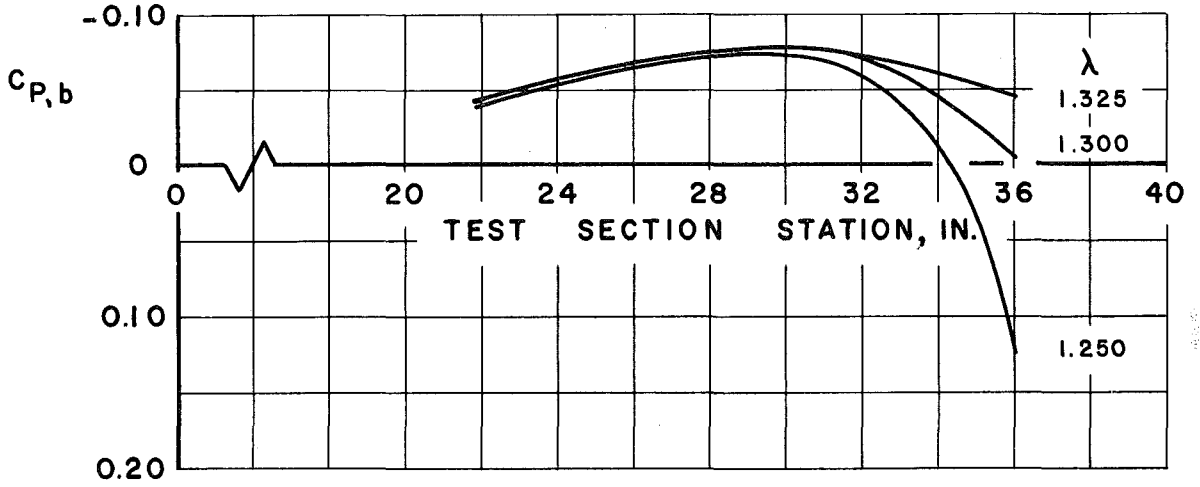


i. Mach Number 1.30

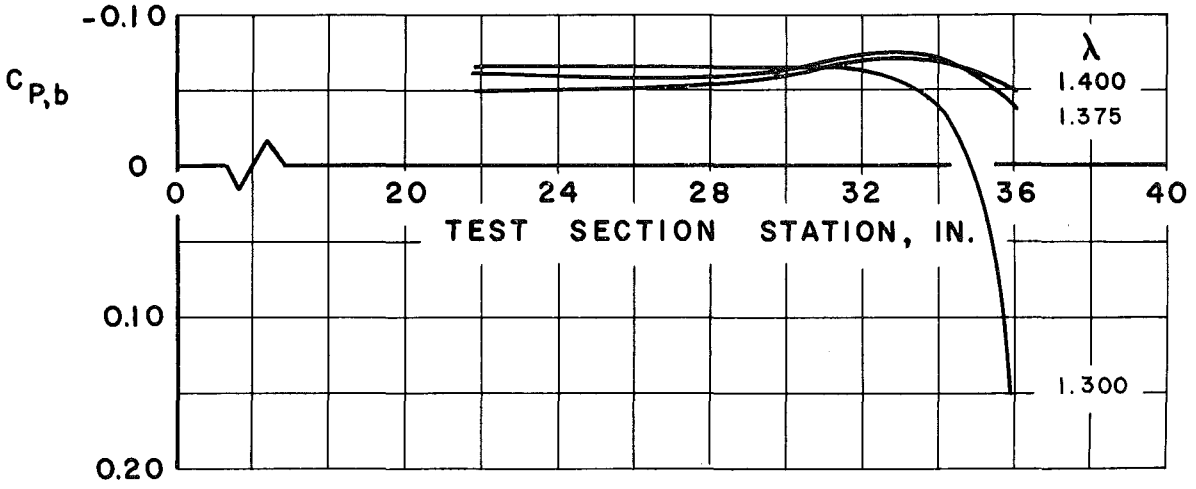


j. Mach Number 1.40

Fig. 17. Concluded

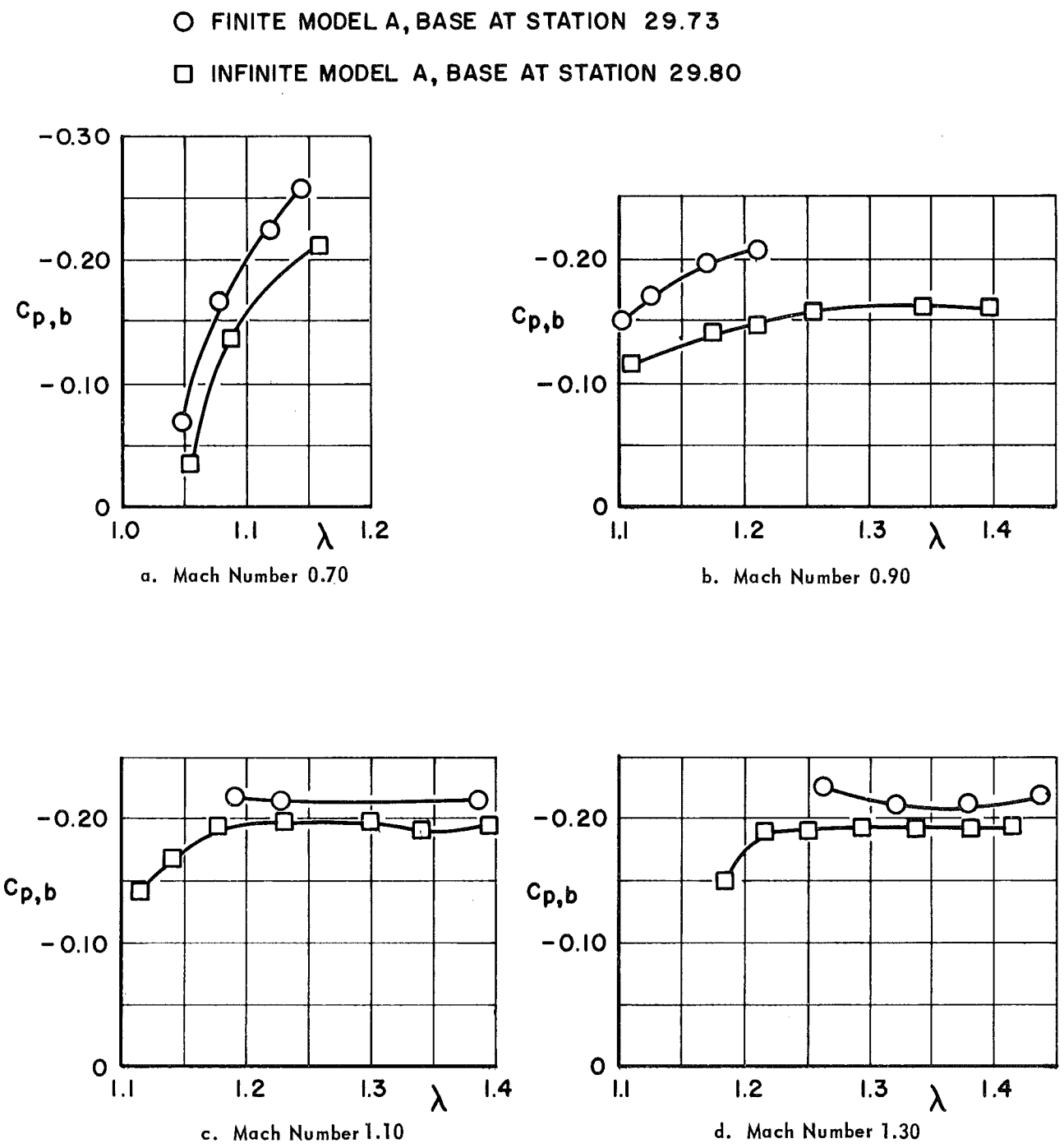


Fig. 18. Comparison of Base Pressure Coefficients Obtained from the Finite- and Infinite- Length Model A

⊙ FINITE MODEL B, BASE AT STATION 29.73

⊡ INFINITE MODEL B, BASE AT STATION 29.75

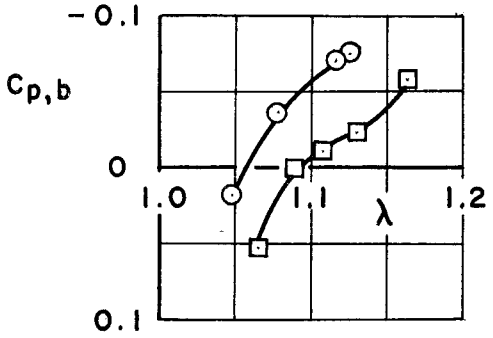


a. Mach Number 0.70

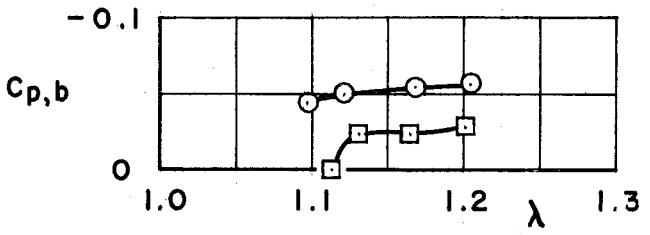


b. Mach Number 0.90

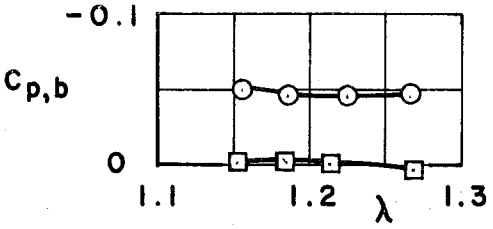


c. Mach Number 1.10

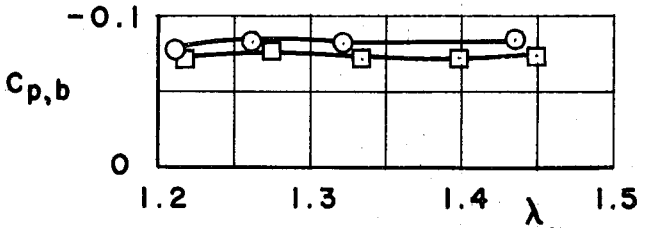


d. Mach Number 1.30

Fig. 19. Comparison of Base Pressure Coefficients Obtained from the Finite- and Infinite- Length Model B